

## Chapter 6

### APPLICATIONS TO RECENT ERUPTIVE EVENTS

#### 6.1 General consideration on Mt.Etna geology, feeding system and eruptive style

Mount Etna is a 3340-m-high complex volcano, extending over about 1250 km<sup>2</sup>, located next to the eastern coast of Sicily at the intersection of two major fault belts trending NNW-SSE (Tindari – Letojanni – Malta) and NNE-SSW (Messina – Giardini) respectively, where three structural domains converge: 1) to the north, the Peloritani mountain range corresponding to the Apennine – Maghrebian overthrust belt, interpreted as related to the collision between the European and African plates; 2) to the south, the little deformed northern margin of the African plate constituted by the Hyblean Mesozoic carbonate succession, which plunges under the Catania – Gela foredeep and the northern range; 3) to the east, the thick sedimentary cover overlying the oceanic Ionian lithosphere. (Fig. 6.1; Cristofolini et al., 1985; Monaco et al., 1997).

The volcanic activity in the Etnean area began ~6-500 ka BP (Condomines et al., 1982; Gillot et al., 1994) with fissural emission of sub-marine and later sub-aerial tholeiitic lavas (dated at ~300 ka BP; Romano, 1982; Kamenetsky and Clocchiatti, 1996; Clocchiatti et al., 1998, and references therein). Later, the erupted products gradually evolved to transitional and finally to Na-alkalic (~200 ka BP; Tanguy et al., 1997, and references therein). The building of central-conduit edifices started about 130-126 ka BP and went on with a sequence of several distinct volcanic centres (De Beni et al., 2005). Their activity was characterized by cycles of prevailingly effusive eruptions, alternated with violent explosive episodes associated to caldera-forming collapses. The “Recent Mongibello” activity (VV.AA., 1979; Romano, 1982), which started ~15 ka BP, displayed a wide range of eruptive styles from effusive and mildly strombolian to sub-plinian. Throughout the recent historical record, and particularly since 1329 AD, the activity was dominated by effusive eruptions from summit craters or parasitic vents on the volcano flanks, often accompanied

by strombolian ejections, with a significantly increased eruption frequency after the benchmark represented by the 1971 eruption (Branca and Del Carlo, 2004). Some of the frequent episodes in the last four decades of activity were important in terms of emission rates and amounts of erupted magma, such as the eruptions of 1983 on the southern flank and of 1991-1993 in the Valle del Bove. Some authors have observed uncommon features of eruptive dynamics during and after the 2001 event, which might be regarded as the most recent benchmark concerning the eruptive behavior (Allard et al., 2006; Viccaro et al., 2006; Ferlito et al., 2008, 2009).

Concerning the structure of the present feeding system, Mt. Etna is characterized by an open-conduit system developed at the intersection of the two main volcano-tectonic structures (the South Rift and NE Rift; defined first in Bousquet et al., 1988 and references therein). The open-conduit system is persistently filled with magma, which undergoes continuous degassing and feeds eruptions from the summit craters. Recent tomography data (Patanè et al., 2003), coupled with previous seismic, deformation, micro-gravimetric and geochemical results, highlighted that magma is injected from the deep portions of the plumbing system (6-15 km) into the more shallow feeding reservoirs (3-5 km of depth). The hypothesis of a dense series of magma batches at 3-5 km of depth, not connected to the surface, matches several geophysical and geochemical evidences (Cristofolini et al., 1985; Patanè et al., 2003; Allard et al., 2006; Viccaro and Cristofolini, 2008). Eruptions fed by magma coming from these reservoirs occur on the volcano flanks, and are generally acknowledged to be more explosive than those from summit craters or subterminal vents (Viccaro et al., 2006; Ferlito et al., 2008, 2009; Corsaro et al., 2009). The occurrence of a mid-crustal magma chamber at depth ranging between 6 and 15 km has been excluded (Cristofolini et al., 1985; Patanè et al., 2003; Allard et al., 2006). Indeed, all the available data support the idea that the structure of the deep plumbing system is made of a plexus of dikes and sills rather than a unique magma chamber.

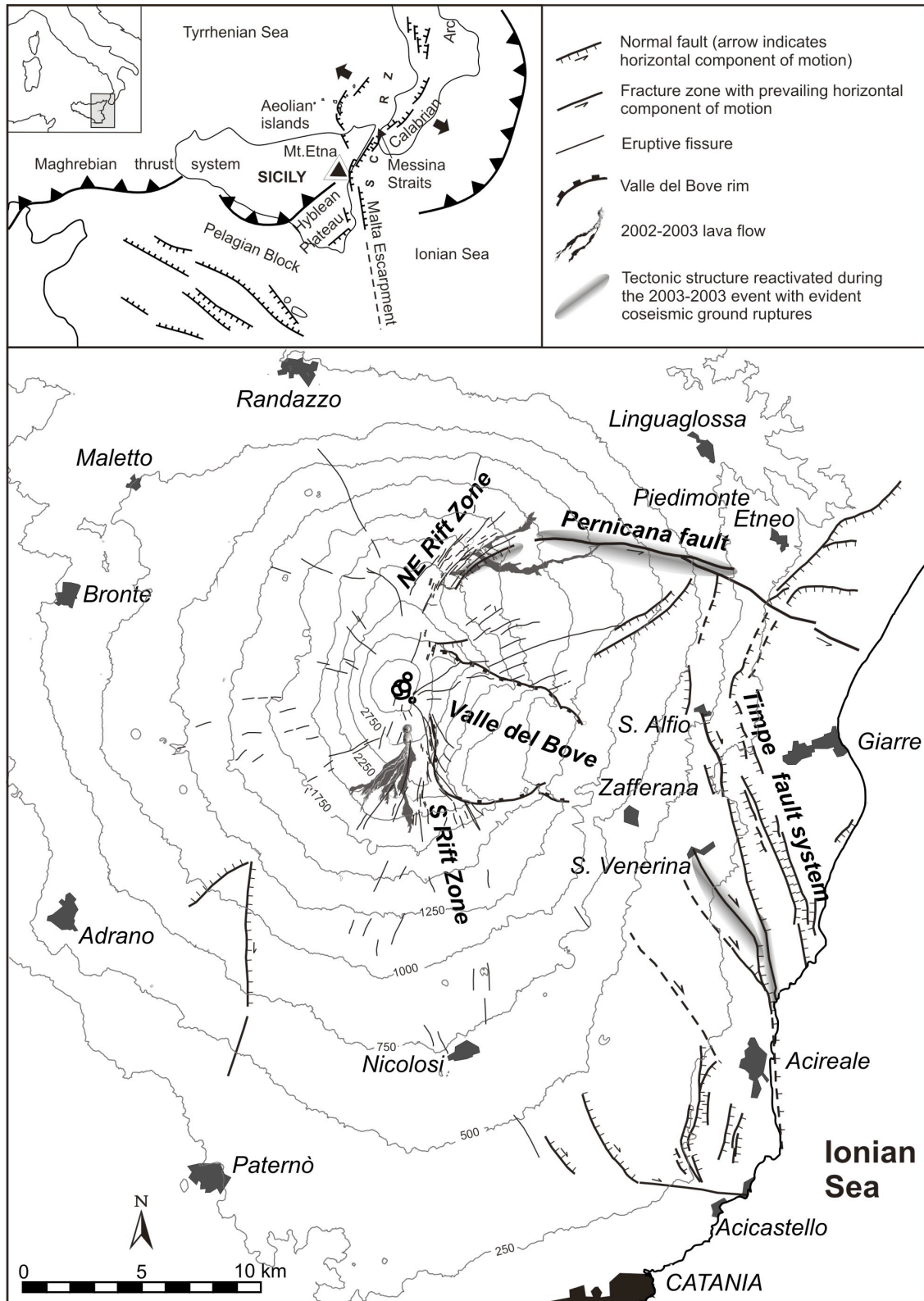


**Fig. 6.1** Map of Mt. Etna volcano with the structural domains involved in active tectonics, major eruptive systems and faults (modified after Viccaro and Cristofolini, 2008).

### **6.1.1 Petrographic and geochemical background**

Historic and recent Etnean lavas widely range in their petrographic features, which mainly relate to phenocrysts abundances. Their porphyritic index (PI, vol%) ranges between 10 and 40, with rare more porphyritic varieties (PI >40). The phenocrysts assemblage is composed of plagioclase zoned from bytownite to oligoclase (~50 vol%), augite (~40 vol%), followed by Fo<sub>70-83</sub> olivine (<7 vol%) and opaque oxides (titaniferous magnetite; <3 vol%; cf. Cristofolini et al., 1987). The presence of scarce amounts (~3 vol%) of amphibole phenocrysts, varying from kaersutite to Mg-hastingsite/pargasite, has been exclusively recognized among the products of the 1763, 1892 and 2001 eruptions (Clocchiatti et al., 2004; Viccaro et al., 2007). Groundmass textures are quite variable: in high scoriaceous levels of lava flows they are hyalopilitic, whereas in the lower ones they tend to be intersertal and holocrystalline. The groundmass is chiefly constituted by labradorite to andesine (~75 vol%), augite (<20 vol%), titaniferous magnetite (<5 vol%) and scarce ~Fo<sub>70</sub> olivine (<3 vol%). Glomerophyric structures are made up of aggregates of augite-olivine plus titaniferous magnetite or plagioclase-augite (Cristofolini and Tranchina, 1980). Textural relations indicate that olivine and titaniferous magnetite are the first crystallizing phases at depth, followed by augite, plagioclase and, if it occurs, amphibole.

Volcanic rocks related to the activity of the last centuries mostly plot in the field of trachybasalts (*s.l.*) on the TAS diagram (cf. Cristofolini et al., 1981; Tanguy et al., 1997). In detail, the historic products fall in the Na-series field and may be defined as hawaiites, whereas the recent ones gradually shift towards a mildly potassic series and may then be defined as trachybasalts (Clocchiatti et al., 1988; Armienti et al., 1989; Condomines et al., 1995; Corsaro and Cristofolini, 1996; Tanguy et al., 1997; Tonarini et al., 2001; Peccerillo, 2005; Viccaro and Cristofolini, 2008). Systematic differences also occur for trace element contents: historic products differ from the recent ones because of their lower concentrations of Rb and Cs and for their slightly higher concentrations of Th, U, Ta, Nb and Zr (Tanguy et al., 1997; Tonarini et al., 2001; Peccerillo, 2005; Viccaro and Cristofolini, 2008). Joined with this, a short-term evolution towards more radiogenic Sr and lower Nd-Pb isotope compositions as well as  $\delta^{18}\text{O}$  was observed. Several hypotheses were suggested to clarify the reasons for this short-term variations, including: 1) a selective contamination by crustal material underlying the volcano (e.g., Clocchiatti et al., 1988; Condomines et al., 1995; Tanguy et al., 1997); 2) the heterogeneous nature of the mantle source (e.g., Armienti et al., 1989; Corsaro and Cristofolini, 1996); 3) a progressive variation due to: a) the contribution of an island-arc component, associated with the southward migration of the Ionian slab (Schiano et al., 2001); b) a metasomatic action of fluids derived from it (Tonarini et al., 2001). The most recent hypothesis

(Viccaro and Cristofolini, 2008) refers these variations to mantle source variably affected by metasomatic influxes, which stabilize variable amounts volatile bearing phases (amphibole± phlogopite). Etnean magmas may therefore originate from heterogeneous domains, which undergo variable partial melting degree constrained at similar T by the amounts of metasomatic phases.

## **6.2 2001 eruptive event**

The 2001 eruption took place mainly in the high southern sector of Mt. Etna with vents from the summit area at the South-East crater and south of the Montagnola, down to 2100 m a.s.l., and later at the Piano del Lago (Fig. 6.3). The eruption was preceded by a large earthquake swarm a few days before its onset and associated to relevant ground deformation and fracture opening. The development of ground cracks along with the hypocentral distribution pattern allowed to define two distinct eruptive systems, simultaneously active to be defined, trending NNW–SSE and N–S, along with a third minor one directed NE–SW (Monaco et al., 2005). Erupted lavas are mainly trachybasalts, with petrological and distinct compositional characteristics, with reference to their vent sites and times of eruption. The eruption produced on the whole an estimated volume of about  $25 \times 10^6 \text{ m}^3$  of lava and  $7 \times 10^6 \text{ m}^3$  of tephra (Behncke and Neri, 2003; Clocchiatti et al., 2004; Lautze et al., 2004). High explosivity, fracture fields with various trends, and two distinct compositions of the erupted magma led several authors to consider the 2001 eruption as among the most relevant of the last years. On the grounds of a detailed and temporally controlled sampling of lavas and tephra, Viccaro et al. (2005) points out that a relationship exists among fracture systems, vent setting and magma compositions, and provide evidence that one of the two magmas could have partially mixed with a third not erupted one. Finally these authors relate the observed changes in the eruptive behavior to the distinct magmas progressively involved in the eruption.

### 6.2.1 Time evolution of the July–August 2001 eruptive episode

The seismic and volcanological events have been described in detail in reports by the INGV-Sezione di Catania reports ([www.ct.ingv.it](http://www.ct.ingv.it)) and in Behncke and Neri (2003). The eruption occurred between July 13<sup>th</sup> and August 9<sup>th</sup> 2001 on the upper slopes of Mt. Etna (Fig. 6.3).

The first eruptive episode, lava fountaining at the South-East crater (July 13<sup>th</sup>), was preceded by a cluster of shallow earthquakes located below the South-East crater area, with their foci distributed between 1.5 km a.s.l. and 2.0 km b.s.l., below the South-East crater area (Alparone et al., 2004). The opening of fractures on the southern slope of the volcano, between 2800 and 2000 m a.s.l., first erupting at their lower end, was heralded by a long-lasting seismic swarm, starting on July 12<sup>th</sup>, with epicentres distributed along a NNW–SSE oriented plane, at depths between 1.5 km a.s.l. and 4 km b.s.l. (Privitera et al., 2001; Bonaccorso et al., 2002; Patane` et al., 2002; Billi et al., 2003; Lanzafame et al., 2003). The

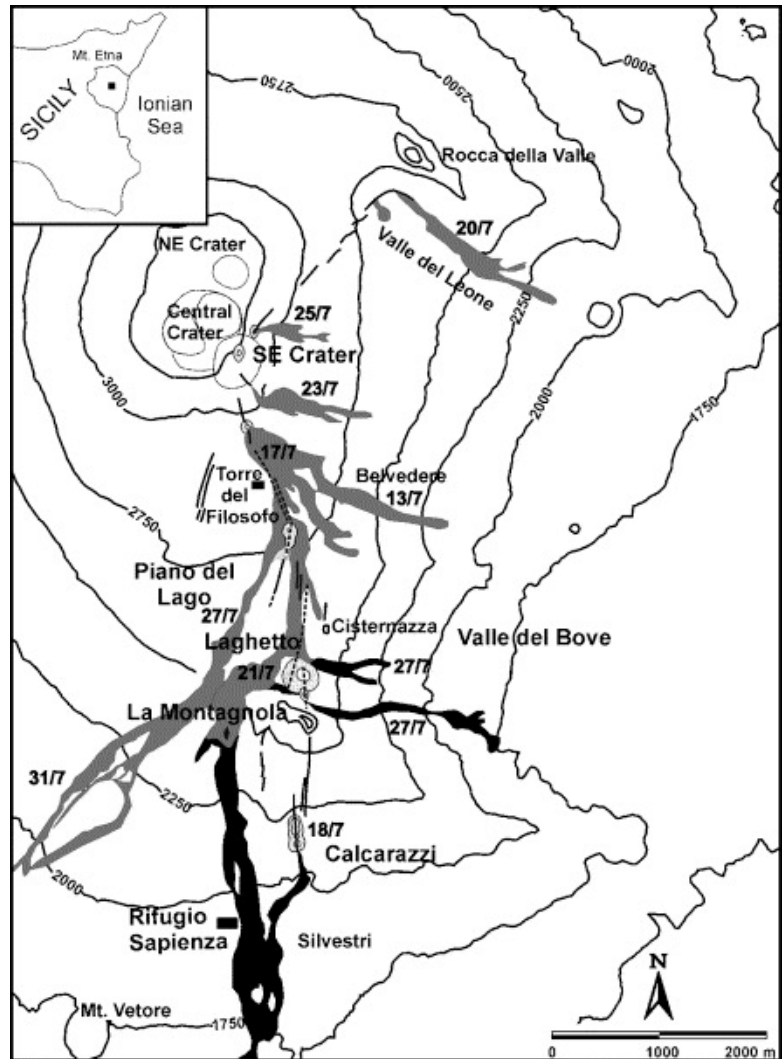


Fig. 6.3 Map of lava field and eruptive fracture of 2001 eruptive event (Viccaro et al. 2005).

The hypocentre distribution vs. time showed a decreasing number of deeper events in the first two days. Later on, from July 15<sup>th</sup> to 18<sup>th</sup> earthquakes were concentrated only within the first 2 km below the surface (Monaco et al., 2005).

On the basis of field observations, the fractures on the southern flank of the volcano have been grouped into two systems: an upper one, from the South-East crater (3000 m a.s.l.) to Piano del Lago, named SE–PL, and a lower one, from Calcarazzi (2100 m a.s.l.) to the Laghetto area (2550 m a.s.l.), named C–L (Viccaro et al. 2005).

### ***6.2.2 The South-East crater–Piano del Lago (SE–PL) system***

The eruption started at the South-East crater on July 13<sup>th</sup>, with lava fountaining related to a little lava flow. On July 13<sup>th</sup> and 14<sup>th</sup>, fractures developed from north to south in the area of Piano del Lago forming a NNW–SSE trending anastomized network that reached the western margin of Valle del Bove (Fig. 6.3). On July 17<sup>th</sup> an eruptive fissure, directed NNW–SSE, which opened at the southern base of the South-East crater, between 3040 and 2940 m a.s.l., with strombolian and effusive activity that resulted in the formation of three aligned spatter spires and a southerly directed lava flow. Ground fracturing propagated downslope between 2900 and 2800 m a.s.l. and formed a NNW trending graben. The lowermost end of this structure propagated in a N15 direction, and reached the Piano del Lago crack field at about 2750 m a.s.l. Along this 600 m long fissure, two groups of driblet cones developed at about 2780 and 2720 m a.s.l., while a well fed lava flow which poured out and expanded in a south-westerly direction down to 2000 m a.s.l.

The night between July 19<sup>th</sup> and 20<sup>th</sup>, activity resumed at the South-East crater; a new set of NE–SW trending fissures opened and the lowermost end of this new fracture system shifted sharply eastwards, where the fractures met the high relief of Rocca della Valle. Lava was emitted from this elbow, at an elevation of 2680 m a.s.l., into the Valle del Leone, with a low output rate ( $<2 \text{ m}^3/\text{s}$ ; Behncke and Neri, 2003).

Finally, on July 23<sup>rd</sup>, a 100 m long NNW–SSE fracture opened on the southern flank of the South-East crater, and a small lava flow came out directed eastwards to the Valle del Bove.

### ***6.2.3 The Calcarazzi–Laghetto (C–L) system***

During the night between July 17<sup>th</sup> and 18<sup>th</sup>, N–S oriented ground fractures opened south of the Montagnola and west of Mt. Calcarazzi at about 2100 m a.s.l. Lava flows were emitted from the lowest portion of these fractures, and advanced southward (Fig. 6.3). Lava crossed the main road to Nicolosi, and flowed east of the Rifugio Sapienza, reaching its lowest elevation (1035 m a.s.l.) seven days later.

In the meanwhile ground fracturing extend northwards from the Calcarazzi area with an overall length of about 1 km up to 2550 m a.s.l., at the Laghetto area (north of the Montagnola). Here the fractures met and intersected the SE–PL ones that were extending southward. On July 21st, a pit crater opened there and ejected mostly ash-laden steam and abundant lithics tephra with spectacularly high thrust columns (about 300 m above the edge of the pit crater) and a convective plume, related to phreatomagmatic explosive activity and conduit widening (Coltelli

et al., 2001; Taddeucci et al., 2002, 2004; Behncke and Neri, 2003). Starting on July 24th, ash and steam emissions evolved to markedly magmatic lava fountaining up to 500 m high. During a two-week period a 120 m high cinder cone was formed through explosive activity. Between July 26<sup>th</sup> and 31<sup>st</sup> lava flowed from the southern base of the new cone down to about 2000 m a.s.l., and destroyed the upper cable-car station and pillars (Calvari and Pinkerton, 2004).

#### **6.2.4. Characteristics of the erupted rocks**

##### **a) Petrography and mineral chemistry**

Petrography and mineral chemistry of SE–PL and C–L lavas have been widely studied; they show markedly distinct textures and modal compositions, which will be only summarized here, for further information see Viccaro et al. (2005).

##### **1) SE–PL Products**

SE–PL lavas are porphyritic (P.I. 30–40) with a seriate texture; their phenocrysts occur in a generally hypocrystalline groundmass (Fig. 6.4A) and are strongly zoned plagioclase, augitic-clinopyroxene, and olivine in volume ratios around 64%, 31% and 5% respectively; Ti-magnetite and apatite are found as accessory phases. The textural relations among the phenocrysts suggest an early crystallization of Ti-magnetite, olivine and plagioclase followed by clinopyroxene.

Plagioclase phenocrysts are strongly zoned (see paragraph 6.2.5 for details) and vary from An<sub>88</sub> at the cores to An<sub>63</sub> at the rims, with low Or (2–4 mol%). FeO<sub>tot</sub> content is notable (0.4–1.03 wt.%), similar to that of other Etnean plagioclases, and higher at phenocrysts cores, probably related to glassy micro inclusions (sieve-texture).

The RE and other minor element analysis of two plagioclase grains were carried out at their rims and cores by Viccaro et al. 2005. The normalized REE patterns (Anders and Ebihara, 1982) are very homogeneous, showing LREE enrichment ( $\Sigma$ LREE=22; La<sub>N</sub>/Sm<sub>N</sub>=16) and marked HREE fractionation (Sm<sub>N</sub>/Yb<sub>N</sub>=10) with Eu/Eu\*=14.

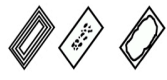
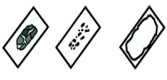

The spider diagram (Anders and Ebihara, 1982) shows high Ba, La, Sr, Ti and Sc values, with positive spikes for Eu, and negative ones for Nb, Zr and Gd (Fig. 4 in Viccaro et al. 2005).

Clinopyroxene compositions fall in the augite field at the boundary with diopside, typically representative of alkali basalt pyroxenes, with a wide range of Al<sub>2</sub>O<sub>3</sub> (3.9–6.9 wt.%)



and SiO<sub>2</sub> (47–50 wt.%) and Al slightly in excess of Si+Al=2. The Chondrite normalized REE patterns (Anders and Ebihara, 1982) of 4 spot analyses are highly homogeneous, with La less enriched than Sm and a strong HREE fractionation (Sm/Yb=5.28).

In the spider diagram (Anders and Ebihara, 1982), the patterns are highly homogeneous with low values of Ba<sub>N</sub>, Nb<sub>N</sub>, Cr<sub>N</sub>, Sr<sub>N</sub>, Zr<sub>N</sub> and Ti<sub>N</sub> whereas Sc<sub>N</sub> exhibits a positive anomaly. Olivine is Fo<sub>76–70</sub>, with scarce tephroite and monticellite components. Fo values are consistent with the range found by Clocchiatti et al. (2004) for olivine in the 2001 lavas erupted from high elevation vents. Ti-magnetite composition is about Mt 48 mol% and Usp 52 mol%. TiO<sub>2</sub> and MgO contents are 13 wt.% and 4.7 wt.% respectively, with Al<sub>2</sub>O<sub>3</sub> up to 6 wt.%.

Emission time	Magma type	Phorphyrific index		Relative proportions of phenocrysts				Plagioclase texture	Type
		Range	Media	Cpx	Ol	Plg	Amph		
SE-PL 3040-2940	HKP	30-40	33.9	31-39	5	55-64	-		Type 1+4+5
EC-L 2620-2320	HKO	10-20	17	40-50	~5	35-45	~6		Type 3+4+5
LC-L 2620-2320	HKO	10-20	17	40-50	~5	35-45	~6		Type 3+4+5

**Table 6.1** Petrographic features of whole rock and classification of recognized plagioclase textures

## II) C–L Products

In C–L lavas P.I. ranges between 10 and 20, with a mesophyric seriate texture; phenocrysts are augitic clinopyroxene (40–50 vol.%), plagioclase (35–45 vol.%), olivine (~5 vol.%), Ti-magnetite (~3 vol.%) and Ca-amphibole (up to 6 vol.%) (Fig. 6.4 B–C). The amphibole is megacrystic (up 10 cm long) and poikilitic, mainly enclosing plagioclase and clinopyroxene. Amphibole crystals are enclosed by a semi-opaque envelope (~0.2 mm thick at maximum), due to dehydration related to eruptive decompression (cf. Clocchiatti and Tanguy, 2001). According to Clocchiatti et al. (2004) these rims are made of a mixture of fassäte, rhönite and anorthite with an interstitial K-rich residual glass. Based on textural features Ti-magnetite, olivine and plagioclase are the first crystallized phases followed by clinopyroxene and finally amphibole. The holocrystalline groundmass is made up of clinopyroxene, plagioclase and olivine with Ti-magnetite and apatite as accessory phases; the total absence of amphibole

microlites must be noted.

Plagioclase phenocrysts core are quite complex in textures and composition ( $\Delta An_{59-75}$ ). Sieve-textures are frequently found and most of the crystals present rims, enriched in An ( $>An_{75-83}$ ) (see paragraph 6.2.5 for details). A thin Na-enriched rim ( $\sim An_{60}$ ) is very often present and the average composition of groundmass plagioclase is  $An_{74}$ . Its  $FeO_{tot}$  content is relatively high (0.54–1.1 wt.%).

RE and other minor element compositions have been analyzed at cores and rims of 4 plagioclase grains by Viccaro et al. 2005. The Chondrite normalized REE patterns (Anders and Ebihara, 1982) of cores are homogeneous, with the exception of one sample, and like those of plagioclase cores in SE-PL rocks. LREE abundances are higher at the cores ( $\Sigma LREE=19-29$ ) than at the rims ( $\Sigma LREE=14-21$ ), whereas core and rim HREE concentrations are similar (0.9–1.9 and 0.8–1.1 respectively).  $Nb_N$  and  $Zr_N$  values are lower in C-L than in SE-PL plagioclase. Clinopyroxene is augite at the boundary with diopside. Crystals are weakly zoned, with the highest  $Mg\#=78$ ; major elements distribution is comparable with that of SE-PL clinopyroxene ( $SiO_2=45-51$  wt.%;  $Al_2O_3=2.7-9.4$  wt.%).

The Chondrite normalized REE patterns (Anders and Ebihara, 1982) for 12 spot analyses show homogeneous core compositions similar to those of SE-PL. At the rims a marked depletion of all REE, Zr, and Y is observed; finally, Cr contents are significantly higher (up to 2000 ppm) than in the cores. These differences are not observed in SE-PL pyroxene.

Amphibole is Mg-hastingsite (Leake et al., 1997; Fig. 6.4C), differing from the kaersutite amphibole of older Etnean volcanics (Cristofolini and Lo Giudice, 1969; Cristofolini and Romano, 1982; Cristofolini et al., 1981, 1988); comparison of the 2001 Mg-hastingsite with

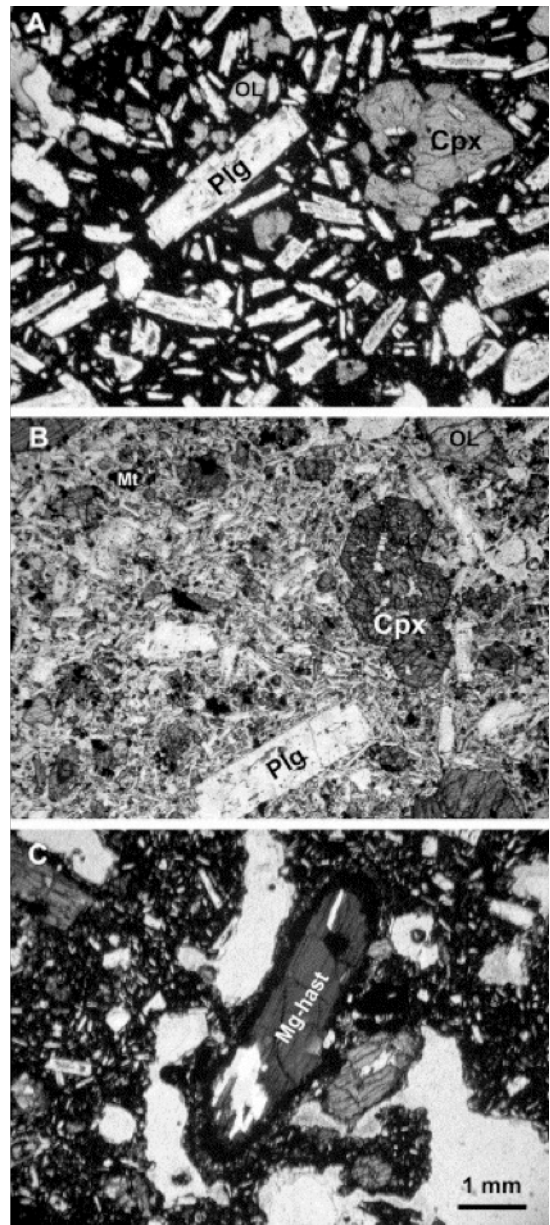


**Fig. 6.4** Optical microscope photographs of A) SE-PL lava, B) C-L lava C) particular o fan amphibole in C-L lava. (From Viccaro et al. 2005)

these kaersutites revealed that the former has lower Na and slightly higher K contents; furthermore, its TiO<sub>2</sub> contents are lower (~3 wt.%), which might be related to a late crystallization of Mg-hastingsite, preceded by Ti-magnetite.

The Chondrite normalized patterns (Anders and Ebihara, 1982) show REE fractionation ( $La_N/Yb_N=4-5$ ), relatively low La (17–23 ppm) and slightly positive Eu anomaly ( $Eu/Eu^*=1.06-1.26$ ). The spider diagram (Anders and Ebihara, 1982) shows LILE slightly fractionated vs. HFSE, enriched Nb, negative anomalies for La and Zr, and very low Cr abundance.

Olivine is weakly zoned ( $Fo_{79-70}$ ), with negligible tephroite and monticellite components. Its forsterite contents are slightly higher than in SE–PL olivine, in accordance with what was defined by Clocchiatti et al. (2004) for olivine in 2001 lavas. Ti-magnetite is made up of Mt 47–65 mol% and Usp 35–56 mol%. TiO<sub>2</sub> and MgO contents are 12.2 wt.% and 3.4 wt.% respectively, with Al<sub>2</sub>O<sub>3</sub> (4.8–5.8 wt.%) slightly lower than in SE–PL Ti-magnetite. On the grounds of the time sequence and vents location of the eruption, the C–L samples have been grouped in Early C–L (EC–L) and Late C–L (LC–L) showing slight but significant chemical differences (see below). Phenocrysts chemistry and modal proportions in the two groups are, however, quite similar.

C–L lavas and tephra have also been characterized by the frequent presence of quartzite xenoliths, with a mosaic granular structure and interstitial silica-rich glass (Corsaro et al., 2004).

### ***b) SE–PL and C–L bulk rock compositions***

The Total Alkali–Silica diagram shows that the rocks from the 2001 eruption plot in the field of the Etnean alkaline suite (Fig. 6.5A; Le Maitre, 1989). They are, however, less sodic than common Etnean rocks, as shown by their K<sub>2</sub>O being higher than (Na<sub>2</sub>O–2), by which they may be defined as mildly potassic (Fig. 6.5B; Le Maitre, 1989). On the whole, the rocks are then potassic trachybasalts, except for two C–L samples, with Alk <5%, erupted at the 2100 m vent of the C–L system, that may be defined as basalts. The primordial mantle (Wood et al., 1979) normalized spider diagrams confirm that minor element compositions of the sampled rocks are generally consistent to those of the basic members of the Etnean alkaline sequence. In detail, they are intermediate between the within plate basalts (WPB) and calc-alkaline basalts (CAB), as defined by Sun (1980) and Pearce (1982). Elements such as Rb, Ba, Th, U and K are enriched in the Etnean rocks compared to the average WPB, whereas Ta, Ti and Nb are less abundant than in common WPB, therefore partly recalling a CAB pattern.

Chondrite normalized (Anders and Ebihara, 1982) REE patterns are markedly homogeneous, with a clear overall fractionation ( $La_N/Yb_N=15-17$ ), and little negative Eu anomaly ( $Eu_N/Eu^*=0.89-0.98$ ); LREE are more fractionated than HREE ( $La_N/Sm_N=3.6-4.0$ ;  $Gd_N/Yb_N=2.7-3.1$ ). On the whole, the pattern is similar to that of the Etnean alkaline suite (Cristofolini et al., 1981, 1984, 1988, 1991; Barbieri et al., 1993; Corsaro and Cristofolini, 1993, 1996; Tanguy et al., 1997).

In spite of their petrographic differences, SE-PL and C-L rocks show an overall limited variability in major and minor element concentrations, with  $SiO_2$  contents in

the range 49–51 wt.%. A careful examination of their variation patterns, however, points out regular changes of the sampled rocks, related to space and time. In particular, the EC-L ones are slightly a.s.l.) of the volcanic edifice; ii) the EC-L magma erupted at lower elevations (2100 m a.s.l.) on the same flank from N-S trending fractures; iii) the slightly different LC-L magma, erupted later from vents at intermediate elevation (2550 m a.s.l.).

All of them are mildly potassic trachybasalts and their plagioclase and clinopyroxene cores have the same REE and minor element contents, supporting the idea of their cognate origin, but appear as fractionated from parent basalts under different physical conditions. SE-PL lavas are porphyritic (P.I. 30–40) with prevailing plagioclase, whereas EC-L and LC-L lavas are mesophytic (P.I. 10–20) with plagioclase and augite in similar amounts and up to 6 vol.% of Mg-hastingsite among the phenocrysts (Table 6.1).

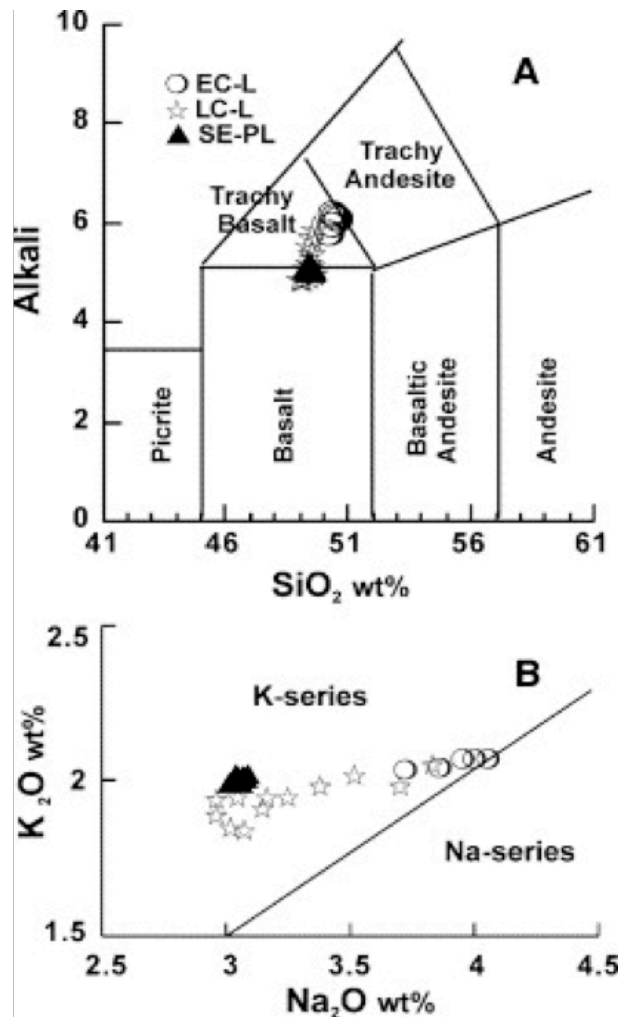


Fig. 6.5 A) TAS of 2001 lavas and tephra; B)  $Na_2O/K_2O$  of erupted juvenile products. (Le Maitre, 1989)

### 6.2.5 Textural and compositional features of plagioclase

Plagioclase in lavas and tephra of 2001 eruption, are mainly euhedral from 0.5 to 2 mm in size. Four different type of textures has been recognized: Type 1, oscillatory zonation; Type 3, patchy cores; Type 4, coarsely sieved cores and Type 5, resorbed dusty rims.

In SE-PL magmas, plagioclase is mainly euhedral with Type 1 textures (Fig. 6.6). Composition vary from  $An_{85}$  at the cores to  $An_{63}$  at the rims, with low Or (2–4 mol%).  $FeO_{tot}$  content is notable (0.4–1.03 wt.%). Some Type 1 crystals have coarsely sieved bytownitic cores (Type 4). Most of the phenocrysts have clear rims but in few cases, resorbed dusty rims (Type 5) are also present. Compositional profiles show that oscillation has an HALF pattern, characterized by cross cutting edges and strong dissolution surfaces. An variations during oscillation is ~5%, and no significant changes in An content are associated to type 4 cores. With type 5 rims is always present an increasing in An and FeO content ( $\Delta An > 10\%$ ).

Plagioclase embedded in E-CL and L-CL magmas present different features textures respect to SE-PL (Fig. 6.7), Type 1 crystals are rare and always shows an HALF oscillatory pattern interrupted by evident dissolution surfaces and convoluted edges. Coarsely resorbed cores (Type 4) are frequent but no significant variation in An and FeO content is evident. Several crystals present Type 3 patchy cores with Type 5 rims (Fig. 6.7) and in many cases, this crystals are quite rounded with a fine glassy rim, testifying a disequilibrium respect to the melt. Strong An increasing (>15-20 % An) is associated to the dusty rim zone.

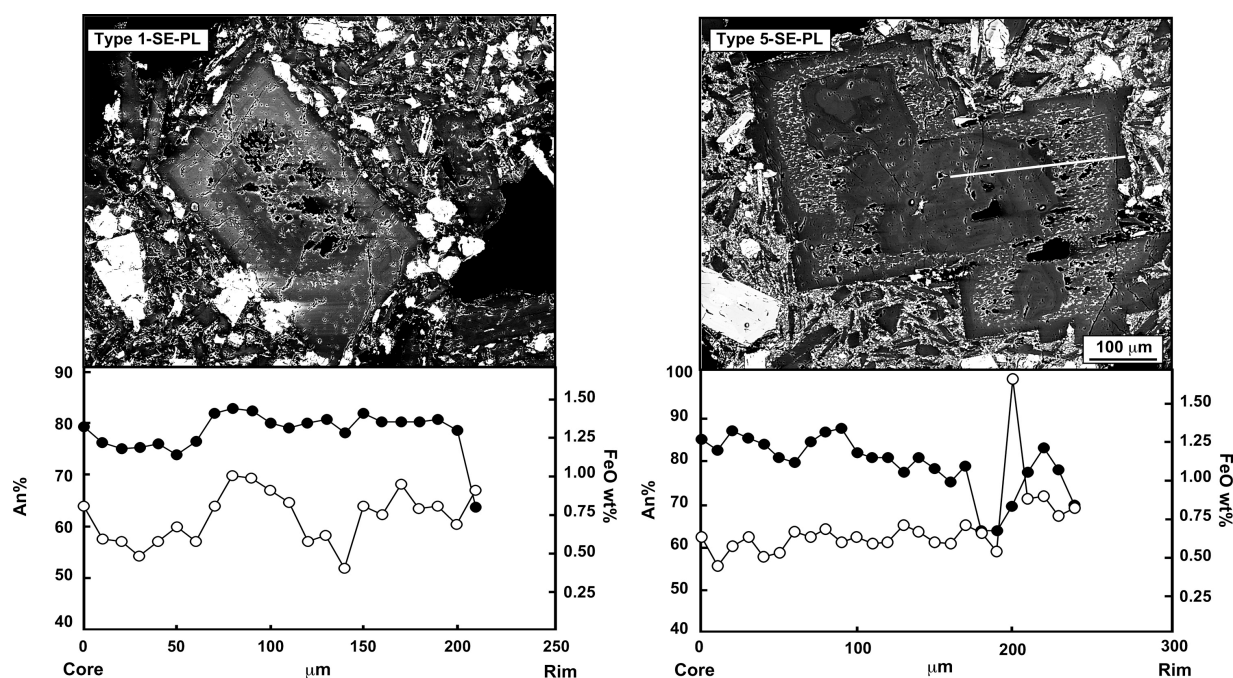


Fig. 6.6 Compositional profiles of An and FeO and SEM photographs of SE-PL plagioclases.

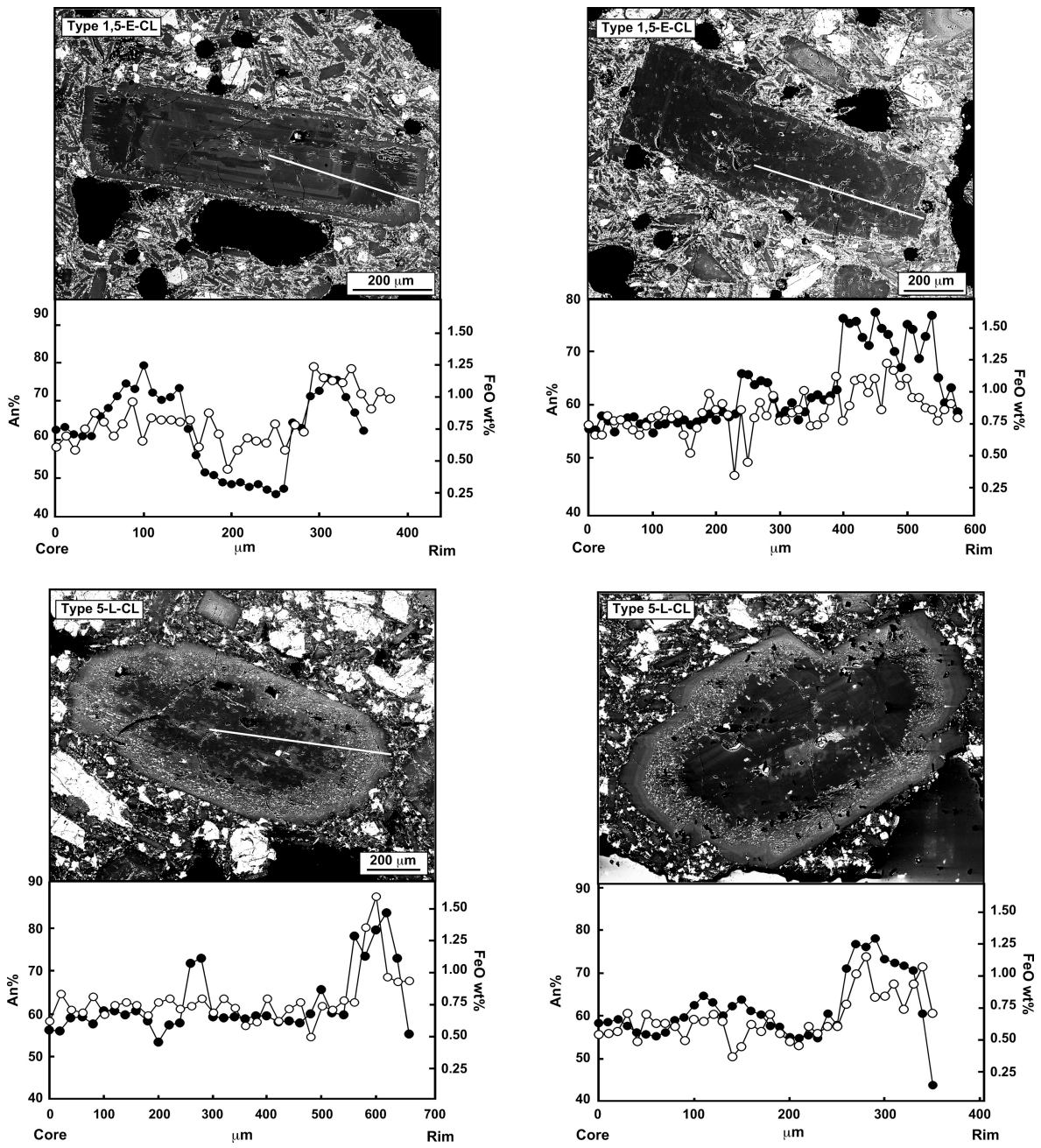


Fig. 6.7 Compositional profiles of An and FeO and SEM photographs of C-L plagioclases.

### 6.3 Eruptive event of 2002/2003

This eruptive event was bilateral, involving simultaneously both southern (S-Rift) and northern (NE-Rift) flanks of the volcano and it has been considered an important chance to study the complex feeding system of Mt. Etna (Ferlito et al. 2009).

On October 26, 2002, at 20:25 GMT a seismic swarm of events (Monaco et al. 2005 and references therein) heralded the opening of eruptive fissures on both northeastern and southern flanks of the volcano. Most of the seismic events had epicenters distributed on the summit area of the volcano. In the first 2 days, seismic activity, initially located below the summit craters, moved northeastwards (Monaco et al. 2005).

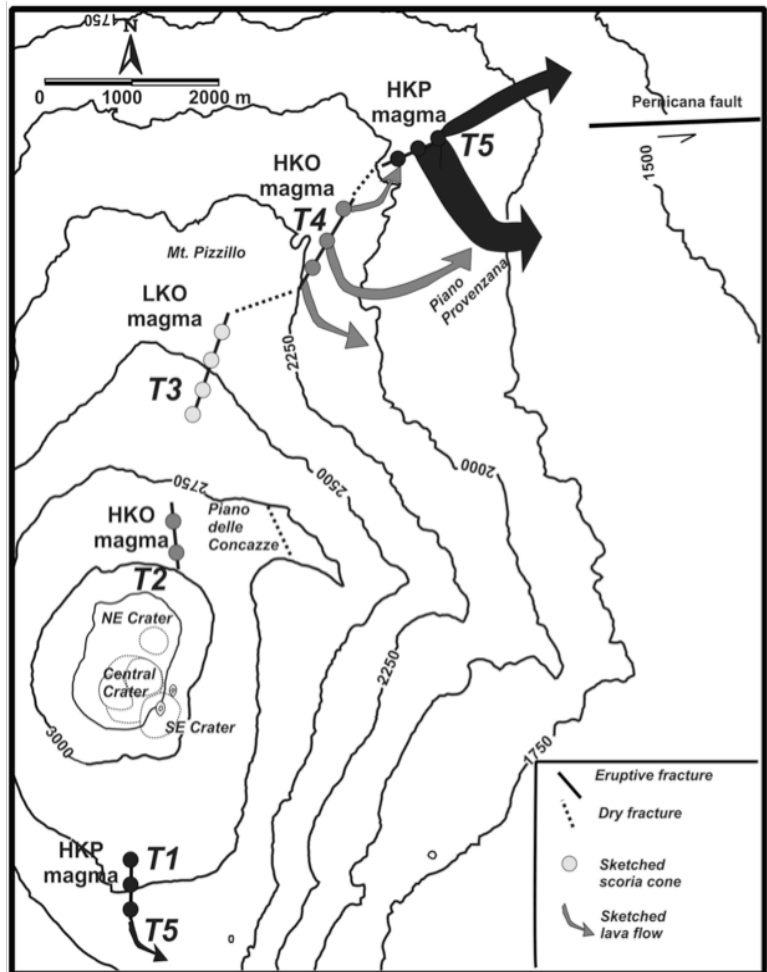


Fig. 6.8. Map of fracture system along NERS and lava emission time. (From Ferlito et al. 2009).

The reconstruction of the exact timing of the fracture opening and the ensuing eruptive activity is mainly based on the I.N.G.V. reports ([www.ct.ingv.it](http://www.ct.ingv.it)) and Andronico et al. (2005), integrated with personal observations from Etna Alpine Guides (Fig. 6.8 and Table 6.2). Accordingly, on October 26 at 22:55 GMT, the eruptive activity started on the southern flank (South Rift System - SRS) with lava fountaining from a N–S-oriented fracture at 2,850–2,600 m a.s.l. (T1, Fig. 6.8 and Table 6.2). Immediately after, at the base of the NE Crater (3,010–2,920 m) an N10W-oriented eruptive fracture had a limited strombolian activity (T2, Fig. 6.8 and Table 6.2). Because of insufficient detail in the timing of the events, T1 and T2 could be coincident. At the same time, and continuing throughout the entire morning of the 27<sup>th</sup> a phreatomagmatic activity occurred in the summit area at the Bocca Nuova and at the Chasm.

The opening of the NE Rift System (NERS) was rather discontinuous, lasted about 12 h and it is described in detailed in Ferlito et al. 2009. It started in the uppermost segment from 2,500 to 2,300 m at 4:45 (GMT) and lasted until 6:45 (T3, Fig. 6.8 and Table 6.2). Here, phreatomagmatic explosions followed by lava fountaining accompanied the fracture opening.

Time	Location	Type of activity	Characteristics of emitted products	Fractures features and orientation
T1 26 Oct 2002 22:55 GMT	SRS 2,850–2,600 m	Lava fountains over 300 m in height	No samples	NS
T2 27 Oct 2002	Northern flank 3,010–2,920 m northeast crater flank	Lava fountains activity lasting about 30 min	Scoriae, HKO magma	N10W
T3 27 Oct 2002 4:45–6:45 GMT	NERS 2,500–2,300 m	Violent Strombolian and phreatomagmatic activity.	Scoriae, LKO magma, Xenoliths occur, mostly trachytic lava	N15E
T4 27 Oct 2002 8:15 GMT	NERS 2,280–2,220 m	Violent Strombolian activity, phreatomagmatic explosions and three lava flows lasted about 2 h. The activity in T3 stopped.	Scoriae and lava flow, HKO magma, Xenoliths occur, mostly plagioclase-rich lava	N35E
T5 27 Oct 2002 12:00–16:00 GMT	NERS 2,050–1,950 m	Strong Strombolian activity and phreatomagmatic explosions. Scoria cones grow around the principal vent at 1,930 m a.s.l. Three lava flows emitted towards the E and NE. The eruptive activity in T4 stopped	Scoriae and lava flow, HKP magma, Quartzarenites xenoliths occur.	N45E
T5 27 Oct 2002 12:00 GMT	SRS 2,850–2,600 m	Intense lava fountain activity. A lava flow was emitted toward the SW	HKP magma, Quartzarenites xenoliths occur.	N-S
T6 12 Nov 2002 12:00 GMT	SRS 2,850–2,600 m	Intense lava fountain and strombolian activity. Lava flow was emitted from the base of a scoria cone at 2,750 m a.s.l.	HKP magma, Quartzarenites xenoliths occur.	N-S
T7 30 Nov 2002 12:00 GMT	SRS 2,850–2,600 m	Several lava flows from 2,750 m a.s.l. directed SSE. Lava fountaining at 2800 m a.s.l produced a new scoria cone.	HKP magma, Quartzarenites xenoliths occur.	N-S
T8 18 Dec 2002 12:00 GMT	SRS 2,850–2,600 m	Strombolian to lava fountaining explosions from the scoria cone at 2800 m a.s.l. Several lava flows directed southwestwards reached 1745 m a.s.l.	HKP magma, Quartzarenites xenoliths occur.	N-S

**Table 6.2** Timing of fracture opening and type of activity of 2002/2003 eruption from Giacomoni et al. Submitted.

The fracturing stopped for less than 2 h and resumed downwards at 8:15 GMT, opening the intermediate segment from about 2,280 to 2,220 m a.s.l. (T4, Fig. 6.8 and Table 6.2). Here, the phreato-magmatic explosions and the lava fountaining were also accompanied by the emission of three lava flows that started at 10:00 GMT. The longest flow reached Piano Provenzana destroying one of the ski lifts of the tourist resort. The lowest segment of the NERS, from 2,050 to 1,950 m, opened between 12:00 and 16:00 GMT (T5, Fig. 6.8 and Table 6.2), with emission of large lava flows which, flowing eastwards, reached Piano Provenzana. However, since the vents on the lowest section were located above a ridge, lava also flowed northeastwards, thus setting fire to the Ragabo pine forest. Noteworthy volcanic activity progressively moved from T1 to T5, where a new segment of the fissure was activated after the emission from the previous segment was over. Immediately after the NERS was entirely activated, the earthquake rate decreased. On October 29, a sharp resumption of the seismic activity was related to the activation of new seismic structures in the southeastern flank of the



volcano. On the northeastern flank, the eruptive activity completely ceased on November 3 and the eruption-related earthquakes continued at decreased rates, ending by November 9 (Barberi et al. 2003; Monaco et al. 2005).

On the southern flank (SRS) lava fountaining and strombolian activity continued from October 26<sup>th</sup> (T1) and began to emit lava flows almost contemporary to the opening of the lowermost segment of the NERS (T5) (Fig. 6.9 and Table 6.2)

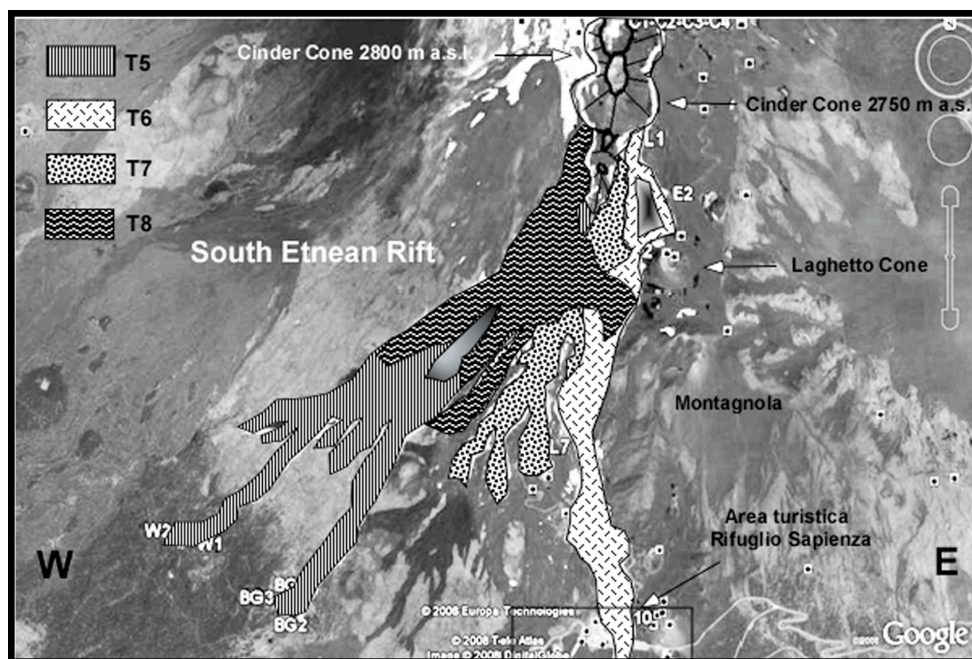


**Fig. 6.9.** Reconstruction of lava field on SRS and emission time of lava flow on a Google Earth satellite image.

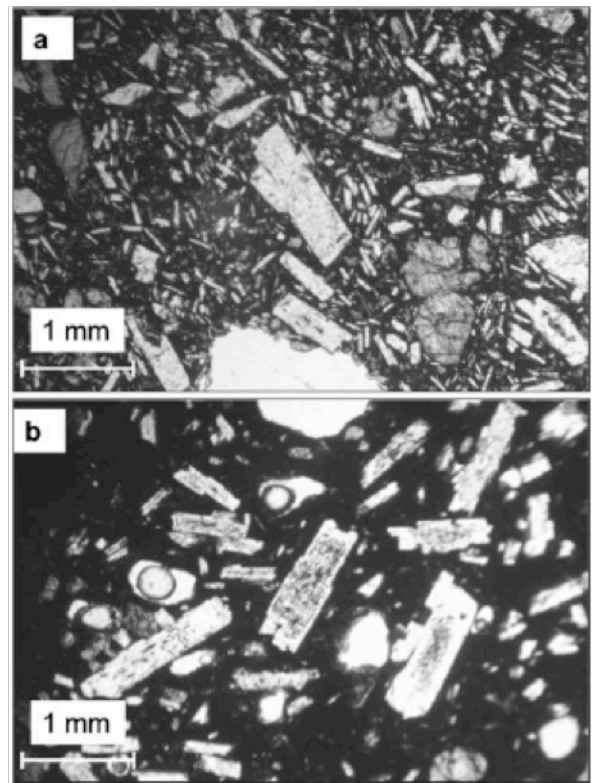
During the following two weeks, the activity at 2750 m a.s.l., was characterized by a subplinian column and wind-carried ashes affected the city of Catania, causing troubles to air traffic and breathing problems. On November 12<sup>th</sup>, the scoria cone located at 2750 m a.s.l. began a strombolian activity and a new lava flow generated from its base (T6) (Fig. 6.9 and Table 6.2). On November 25<sup>th</sup> a decrease in explosive activity and effusion rate was reported (T6). On November 30<sup>th</sup> the activity resumes (T7) (Fig. 6.9 and Table 6.2) with several lava flows emitted from the cone at 2750 m a.s.l. and directed to the SSE. At the same time, strong lava fountaining at 2800 m a.s.l produced a new scoria cone, bombs, lapilli and ashes, completely buried “Torre del Filosofo” hut (T7). The activity remained almost stationary until December 18<sup>th</sup> when it increased with strombolian to lava fountaining explosions from the cone at 2800 m a.s.l. (T8) and several flows directed southwestwards reached 1745 m a.s.l. and overlapped until January 28<sup>th</sup> when eruption ended (Fig. 6.9 and Table 6.2).

### 6.3.1 Petrological features of the erupted rocks

All samples have been analyzed for whole-rock major and trace elements using X-ray fluorescence (Thermo ARL Advant XP). Intensities have been corrected for matrix effects using the method of Lachance and Trill (1966). Loss on ignition (L.O.I.) has been determined by gravimetric method assuming  $\text{Fe}_2\text{O}_3$  as 15% FeO. The most representative samples have been selected for REE analyses by means of ICP-MS (Plasma Quad 2Plus VG Elemental). Both major and trace element analyses were carried out at the Department of Earth Sciences of the University of Ferrara (Italy). Porphyritic Index (P.I.) has been determined through a Scion Corporation image elaboration program ([www.scioncorp.com](http://www.scioncorp.com)) (Table 6.3). Major elements in the mineral phases were analyzed using electron microprobe (EMP) at the Padova section of the CNR Institute of Geosciences and Georesources (IGG) (Italy).









All the collected juvenile rocks can be defined as trachybasalts and trachyandesites (Le Maitre 2002) with  $\text{SiO}_2$  ranging between 48 and 52 wt%. Petrographic features are: porphyritic texture with phenocrysts of plagioclase, diopsidic to augitic clinopyroxene (Morimoto 1988), olivine and Ti-magnetite set in a microcrystalline to cryptocrystalline and glassy groundmass. Based on petrographical (P.I.) and geochemical features (mainly  $\text{K}_2\text{O}$ , Rb and Nb), three groups of emitted products have been distinguished: (1) High-K Porphyritic (HKP) group with high potassium contents ( $\text{K}_2\text{O} > 2$  wt%) and P.I. ranging between 20 and 32%; (2) High-K oligo-phyric (low-phyric) (HKO) group with high-potassium content ( $\text{K}_2\text{O} > 2$  wt%) and P.I. ranging between 10 and 18%; (3) Low-K oligo-phyric (low-phyric) (LKO) group with low potassium content ( $\text{K}_2\text{O} < 2$  wt%) and P.I. between 10 and 17% (Table 6.3).

**High-potassium porphyritic volcanics (HKP).** Volcanics of this group are both lava flows and tephra, emitted by the lower segment of the NERS, during T5 and by the SRS during the entire eruption.



**Fig. 6.10** a) Photomicrographs of HKP lava. The groundmass is microcrystalline texture. b) Photomicrographs of large plagioclase phenocrysts in a glassy groundmass in LKO lava.

Samples emitted at the NERS display porphyritic texture, P.I. between 20 and 32%, with a generally microcrystalline groundmass. Phenocrysts are strongly zoned plagioclase, diopsidic clinopyroxene and olivine in volume ratios of about 60, 30, and 10%, respectively (Fig. 6.10a and Table 6.3); Ti-magnetite and apatite are found as accessory phases. K<sub>2</sub>O content ranges between 2.02 and 2.23 wt%, while MgO content shows variability from 4.03 to 4.98 wt% (Fig. 6.11). These products present lower contents in La, Nb, Ba, U and Th, and ratios of K/Nb, K/Th, etc., generally higher than those of the LKO products (Ferlito et al. 2009). Fo content of olivine ranges between 78.1 and 74.5, and no zoning was observed. Clinopyroxene composition falls in the diopside field (Morimoto 1988), with variable contents of Al<sub>2</sub>O<sub>3</sub> (3.55–7.68 wt%), SiO<sub>2</sub> (43.1–49.6 wt%) and TiO<sub>2</sub> (1.35–1.41 wt%). Dm-size sedimentary xenoliths of quartzarenites have been found. (Ferlito et al. 2009).

Emission time	Magma type	Porphyritic index		Relative proportions of phenocrysts			Plagioclase texture	Type
		Range	Media	Cpx	OI	Plg		
T2 N	HKO NE	12	12	35-40	10-15	35-40		Type 2+6
T3 N	LKO	10-17	12.2	30-35	10-15	45-55		Type 2/3+6
T4 N	HKO	11-18	15.3	30-35	10-15	45-55		Type 2+6
T5 N	HKP	20-32	23.9	30-35	10-15	50-60		Type 2+6
T5 S	HKP	21-28	22.8	50-55	5-15	25-40		Type 2
T6 S	HKP	18-35	23.6	40-50	10-15	25-40		Type 1
T7 S	HKP	18-31	23.8	40-50	10-15	25-40		Type 1
T8 S	HKP	19-19.4	19	45-50	20-25	10-15		Type 1+5

**Table 6.3.** Petrographic and petrological feature of emitted products of 2002/2003 eruption. Plagioclase texture types are also reported.

Samples emitted on the SRS are all trachybasalts with SiO<sub>2</sub> and K<sub>2</sub>O varying from 48.14 to 49.97 wt% and from 2.02 to 2.21 wt%, respectively. Rather high MgO content (6.37-5.23) and Mg# (56.47-53.24) reveal a quite primitive features for the lavas emitted on the SRS, also compared to those emitted on the NERS that are more differentiated (mg# 55.25-51.81). (Fig. 6.11 and 6.12)

The reconstruction of the magma evolutionary trend could not take into account the petrological features of the earliest products emitted on the SRS at T1, buried by younger products. Lavas and tephra sampled in the highest layers of the same scoria cones were thus assigned to T5 (from October 26<sup>th</sup> to 12 November 12<sup>th</sup>). They have P.I. of 21-28% with Cpx

50-55%, Plg 25-40% and Ol 5-15% (Table 6.3); Mg# varying from 56.47 to 54.69, representing the most primitive samples erupted during the event. Magmatic products outpoured on T6 shows a changing in composition, shifting clearly to more primitive features and on T7 they are progressively more evolved, passing from 55.07 to 53.24 Mg# (Fig. 6.12). Petrographic features remain almost constant, with slightly changes of the P.I. (20,9-35%) and modal proportions of Cpx 40-50%, Plg 25-40%, Ol 10-15% (Table 6.3). Finally at T8, lavas present again primitive features (Fig. 6.12). They are less porphyritic (P.I. 19%) with Mg# varying from 55.73 to 54.18, and are characterized by large clinopyroxene (Cpx, 45-50 vol%), olivine (Ol, 15-20 vol%), and small plagioclase (Plg, 15-20 vol%) crystals (Table 6.3).

#### High-potassium oligo-phyric

#### volcanics (HKO).

HKO products have been emitted by small vents at the base of the NE crater during T2 and by the intermediate section

of the NERS, between 2,280 and 2,220 m a.s.l., during T4. Lavas with comparable features have been reported as emitted at the southern flank, at the beginning of the event (Andronico et al. 2005). These lavas and tephra are characterized by low-modal phenocrysts abundance, with P.I. between 11 and 18% and highly vesiculated. Phenocrysts are plagioclase, diopsidic to augitic-clinopyroxene, olivine and Ti-magnetite in volume ratios of about 55, 30, 10 and 5%, with a generally glassy groundmass. Ratios of about 50, 35, and 15% of plagioclase, clinopyroxene and olivine characterize the samples from the southern flank (Table 6.3). These

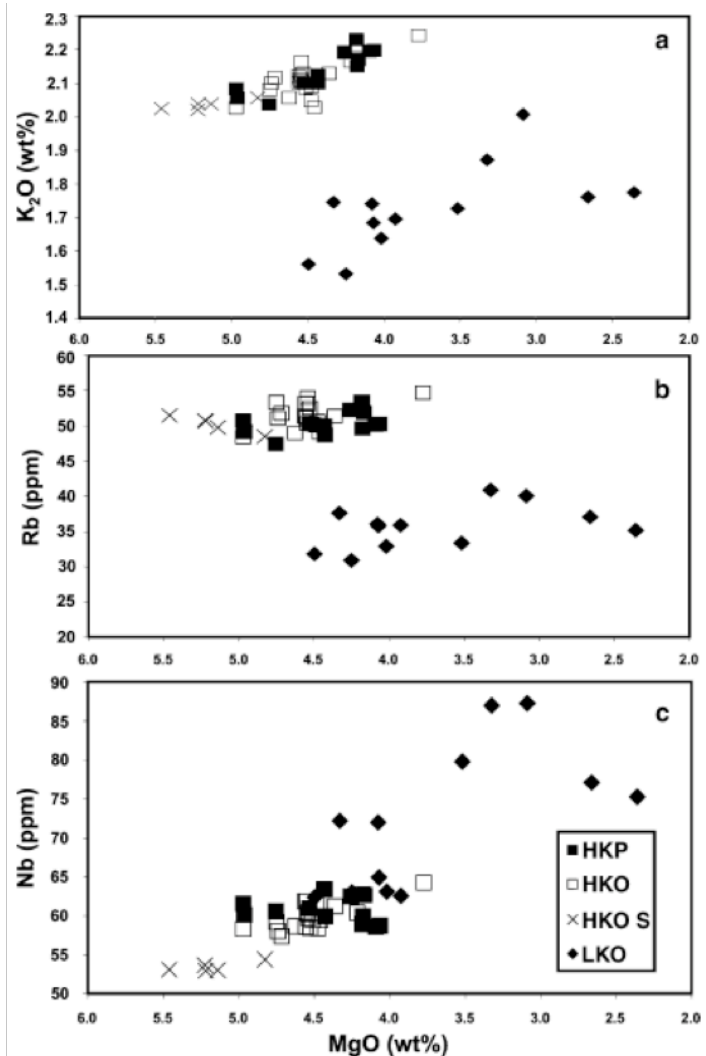


Fig. 6.11 K<sub>2</sub>O (a), Rb (b) and Nb (c) vs. MgO variation diagrams. HKP, high-potassium, highporphyritic products; HKO, high-potassium oligo-phyric products; HKO S, highpotassium oligo-phyric products sampled on the southern (S) flank of the volcano; LKO, low potassium oligo-phyric products. MgO and K<sub>2</sub>O in wt%; Nb and Rb in ppm.

products have major and trace element contents closely comparable to those of HKP, with MgO between 3.77 and 4.97 wt% (excluding HKO S, Fig. 6.11). Consequently, primordial mantle-normalized trace-element patterns show similar trends (Ferlito et al. 2009). Olivine presents Fo between 75.5 and 79.9. Clinopyroxene is mainly diopside (a few augitic compositions have also been found) with Al<sub>2</sub>O<sub>3</sub> content varying between 2.71 and 5.00 wt%, SiO<sub>2</sub> values between 48.8 and 50.8 wt% and TiO<sub>2</sub> content between 1.13–1.48 wt%. Xenoliths of plagioclase-rich trachyandesitic lavas, locally named “Cicirara” and, in less abundance, banded trachites, have frequently been found in these NERS lavas, whereas only quartzarenites xenoliths have been found in the HKO lavas emitted by the N–S fracture on the southern flank. According to Le Maitre (2002) HKP and HKO products can be classified as potassic trachybasalts.

**Low-potassium oligo-phyric volcanics (LKO).** The LKO products have been exclusively emitted from the upper section of the fracture system, between 2,500 and 2,300 m a.s.l. This group is formed only by tephra with low modal phenocrysts abundance (P.I. 10–17) and glassy groundmass (Fig. 6.10b and Table 6.3). The phenocrysts are zoned plagioclase, clinopyroxene and olivine in volume ratios of about 55, 35, and 10%, respectively (Table 6.3). Ti-magnetite is found as an accessory phase. K<sub>2</sub>O content is always lower than 2 wt% with MgO contents between 2.36 and 4.50 wt% (Fig. 6.11). According to Le Maitre (2002), these products may be defined as hawaiites. Compared to HK magmas, LKO products generally show higher La, Nb, Ba, U, Th and lower ratios of K/Nb, K/Th, etc. (Ferlito et al. 2009). Fo contents in olivine vary from 69.9 to 74.8. Clinopyroxene is diopside with Al<sub>2</sub>O<sub>3</sub> variable between 4.03–6.71 wt% and TiO<sub>2</sub> between 1.10–1.83 wt%. Plagioclase An content varies between 52.0 and 86.2 wt% and reverse zoning is common (See paragraph 6.3.2 for details).

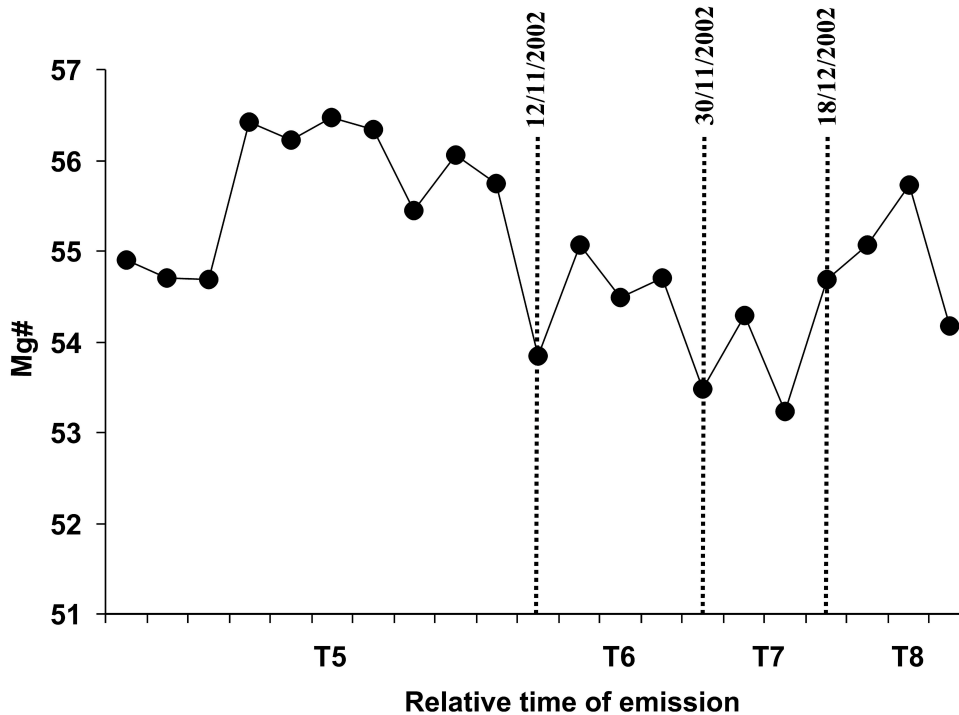


Fig. 6.12 Mg# versus relative time of emission of magma from the SRS. From Giacomoni et al. (Submitted).

### 6.3.2. Textures and composition of plagioclases of 2002 eruption

Although all the textures described in Ch. 3 are recognizable on 2002 products, only four of them are the most commons and really distinctive of the erupted magma: plagioclase with oscillatory zonation (Type 1), plagioclase with dissolved or resorbed cores (Type 2), plagioclase with resorbed dusty rims (Type 5) and plagioclase with melt inclusions at the rim of the crystal (Type 6) (Table 6.3).

Plagioclase in LKO magma presents two textures type: type 2, dissolved cores and type 3, patchy cores (Fig. 6.13a,b). Dissolved cores are clear and bytownitic in composition ( $An_{82-88}$ ). Chemical variations constitute an oscillatory zonation, mostly discordant with FeO, towards more sodic contents (Fig. 6.13a). Patchy cores are labradoritic ( $An_{70-80}$ ), chemical zoning inside this core, is quite concordant with FeO (Fig. 6.13b) Both crystals with dissolved (type 2) and patchy (type 3) cores are followed by a more sodic overgrowth with similar chemical composition. Rims are mostly oscillatory, with a LAHF zoning pattern ( $An_{60-70}$ ).

Plagioclase in HKO and HKP N magmas erupted from the intermediate and lower segment of the NERS (T4 and T5) have highly anorthitic ( $An_{91-77}$ ) dissolved rounded cores (Type 2) enclosed by an andesinic ( $An_{41}$ ) overgrowth (Fig 6.14a), with dense stripes of melt inclusion (Type 6) parallel to the crystallographic planes. An compositional profiles underline

two important An decrease in correspondence of the stripes of melt inclusion and at the outermost rim of the crystal not accompanied by abrupt decrease of FeO (Fig. 6.14c).

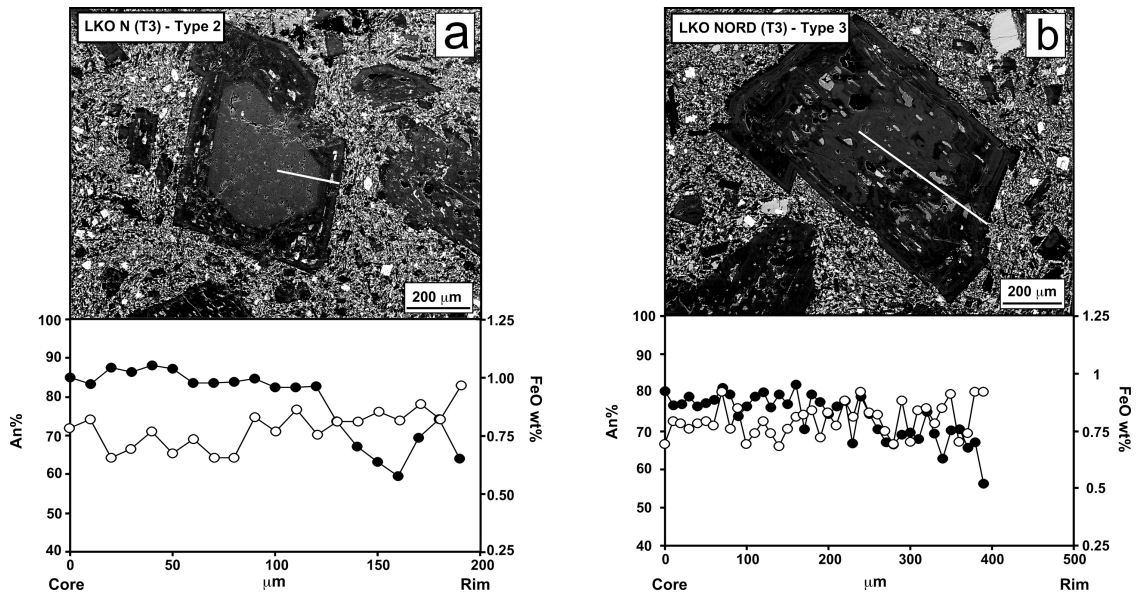


**Fig. 6.13** SEM images and compositional profiles of An and FeO of plagioclase in LKO magmas. **a)** dissolved rounded Type 2 core; **b)** patchy core Type 3.

Lavas erupted on the southern flank (SRS) at T5 present textural features of plagioclase strictly comparable with those emitted on the northern flank. In fact the former present dissolved (Type 2) or coarsely sieved cores (Type 4) and rims characterized by oscillatory zonation (Fig 6.14b). Compositional profiles evidence bytownitic dissolved and rounded cores ( $An_{87-80}$ ) and abrupt decreases of An ( $\sim 30\%$  An) content (Fig 6.14b). Plagioclases contained in lavas emitted at T6 are characterized by coarsely sieved core (Type 4) and resorbed dusty rims (Type 5). Chemical profiles evidence bytownitic cores ( $An_{71-80}$ ) in Type 4 crystals and an increase in An and FeO contents associated to the resorbed dusty rims.

Lavas erupted at T7 contain crystals which are bytownitic ( $An_{76-84}$ ) to andesinic ( $An_{53-66}$ ) with oscillatory zonation or coarsely sieved cores (Type 4). Compositional profiles evidence a quite homogeneous An content in the cores and an abrupt decrease close to the rim of crystals.

Plagioclases embedded in lavas emitted at T8 are bytownitic to labradoritic ( $An_{55-80}$ ) in composition with crystals with resorbed dusty rims (Type 5) and coarsely sieved cores (Type 4). An and FeO profiles evidence an abrupt increase in both An and FeO content associated to dusty resorbed rims (Fig. 6.14d)

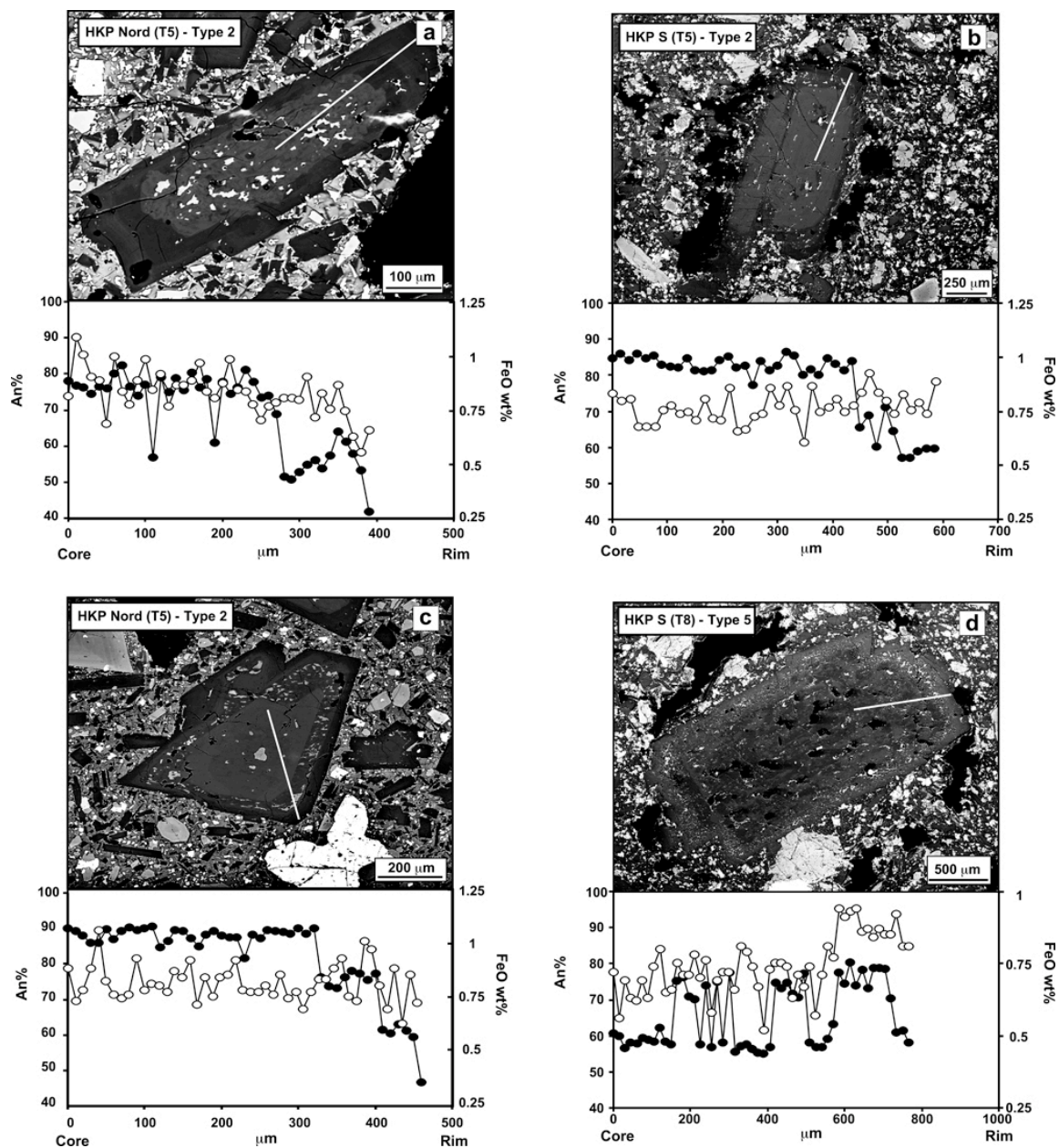


Fig. 6.14 Core-rim profile of An and FeO for HKP magmas emitted from NERS and SRS

Trace elements determinations have been performed on the plagioclase of 2002/2003 eruption, by laser ablation coupled with plasma-mass spectrometry (LA-ICP-MS) at the CNR institute of Pavia. In Fig. 6.15 Sr/Ba ratio is reported as average of three measurements from core to the crystals rim of LKO (Fig. 6.15a,b) and HKP (Fig. 6.15c,d) erupted from the NERS. Sr/Ba has been selected as a good indicator of a change in the melt composition, due to the difference in the partition to the solid between Sr and Ba (Blundy and Wood, 1991). Sr/Ba ratio in LKO is present different values between type 3 and type 2 phenocrysts. In Type



3 patchy cores phenocrysts, Sr/Ba ratio is 10.798 in the cores; it reduces after the convoluted edge of the core (Sr/Ba=8.182) and increases at the crystal rims (Sr/Ba=10.644) (Fig. 6.15a). In type 2, dissolved cores phenocrysts, Sr/Ba ratio is quite higher at the crystal cores (Sr/Ba=23.182) and it remains mostly constant at the overgrowth after dissolution (Sr/Ba=23.095) and it drops at the outermost crystal rims (Sr/Ba=8.161) (Fig. 6.15b).

Sr/Ba ratio in HKP phenocrysts present some differences between type 2 and type 6 plagioclases only at the crystals rim. Sr/Ba values are quite constant varying between 22.115-22.669 at the cores, and 22.393-22.476 at the crystal middle. At the rims, type 2 plagioclase show a drop to Sr/Ba=18.772, while in type 6 plagioclases, this drop is much abrupt, and Sr/Ba ratio is 6.234.

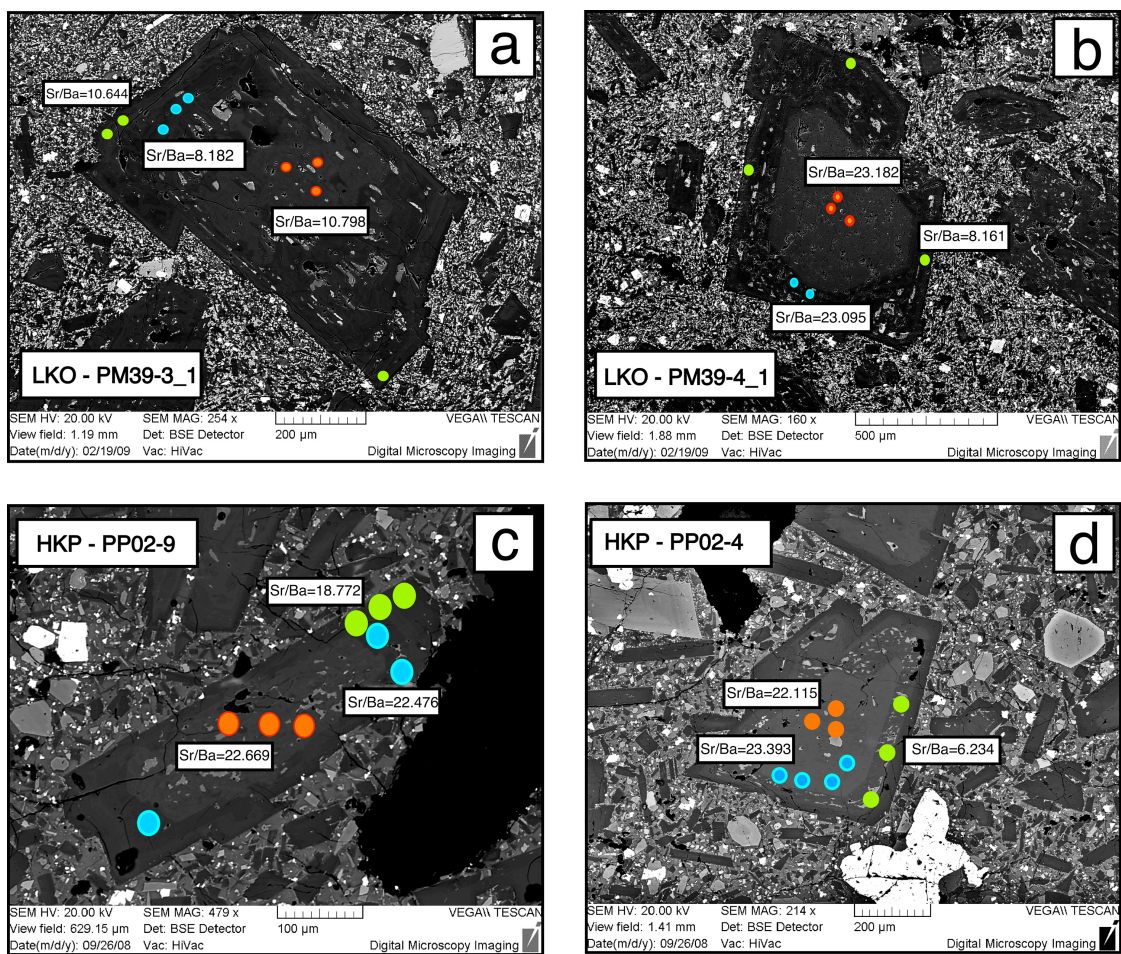


Fig. 6.15 Sr/Ba ratio of LKO and HKP magmas erupted on NERS.

Sr/Ba ratio in HKP lavas erupted on southern flank (SRS), differ to respect of the emission time. Type 2 plagioclases erupted on T5, almost simultaneously with the NERS, have ratios similar to those of the NERS, Sr/Ba=22.892 at the cores. At the overgrowth around the cores it remains quite constant (Sr/Ba=22.211) and show an abrupt decrease Sr/Ba=18.211 at the

crystal rim (Fig. 6.16a). Plagioclase emitted during T6 has Sr/Ba ratio almost, it varies from Sr/Ba=15.076 at the core, Sr/Ba=17.602 in middle and Sr/Ba=16.678 at the rim (Fig. 6.16b). Coarsely sieved, type 4 phenocrysts, embedded in lavas emitted on T7, show a decrease in Sr/Ba content from core to rim, shifting from Sr/Ba=17.367 to Sr/Ba=10.070 respectively (Fig. 6.16c). Type 5 resorbed dusty rims plagioclase, emitted on T8, shows an increment of Sr/Ba ratio from core to rim, passing from Sr/Ba=10.862 to Sr/Ba=21.374 at the rim (Fig. 6.16d).

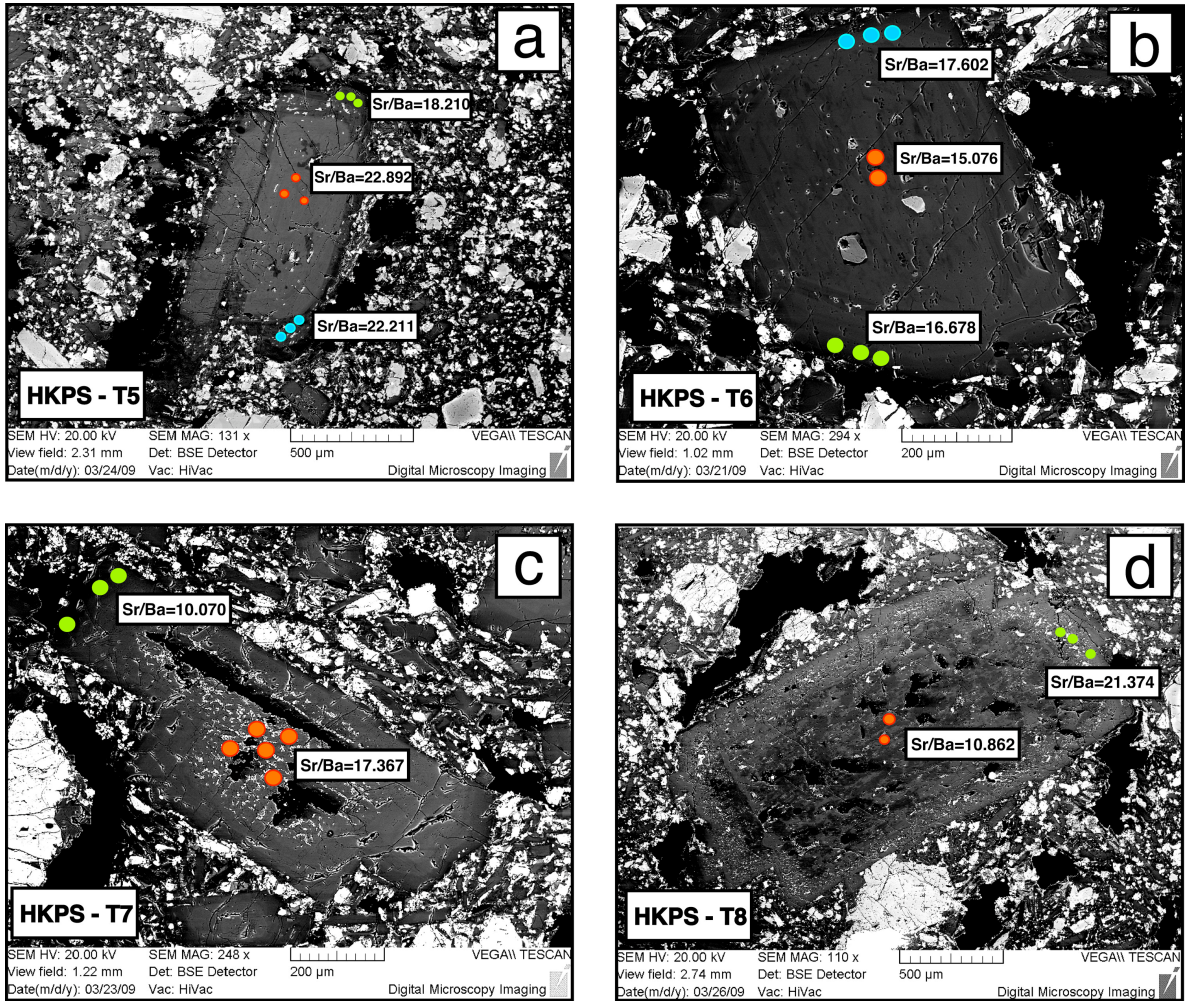


Fig. 6.16 Sr/Ba ratio of plagioclases from HKP magmas emitted on SRS fracture system.

## 6.4 Eruptive event of 2004/2005

After the 2001 and 2002/2003 spectacular lateral eruption, Mount Etna activity resumed after 20 months of quiescence, on September 7<sup>th</sup> 2004 and lasted for about 6 months. Its onset was not heralded or accompanied by short-term precursory signals, such as seismicity and ground deformations, and neither by explosions at the summit craters (Burton et al. 2005). The event started on September 7<sup>th</sup>, when a complex fracture zone extended ESE (Fig. 6.17) from the Southeast Crater (SEC) toward the rim of Valle del Bove over a length of about 200 m. A small SE directed lava flow poured out at 2,920 m a.s.l. and stopped a few hours later. On September 9<sup>th</sup>, a portion of the fracture zone collapsed at 2,820 m a.s.l and a pit was formed, emitting dense white vapors and occasional bombs and lapilli on September 13<sup>th</sup>.

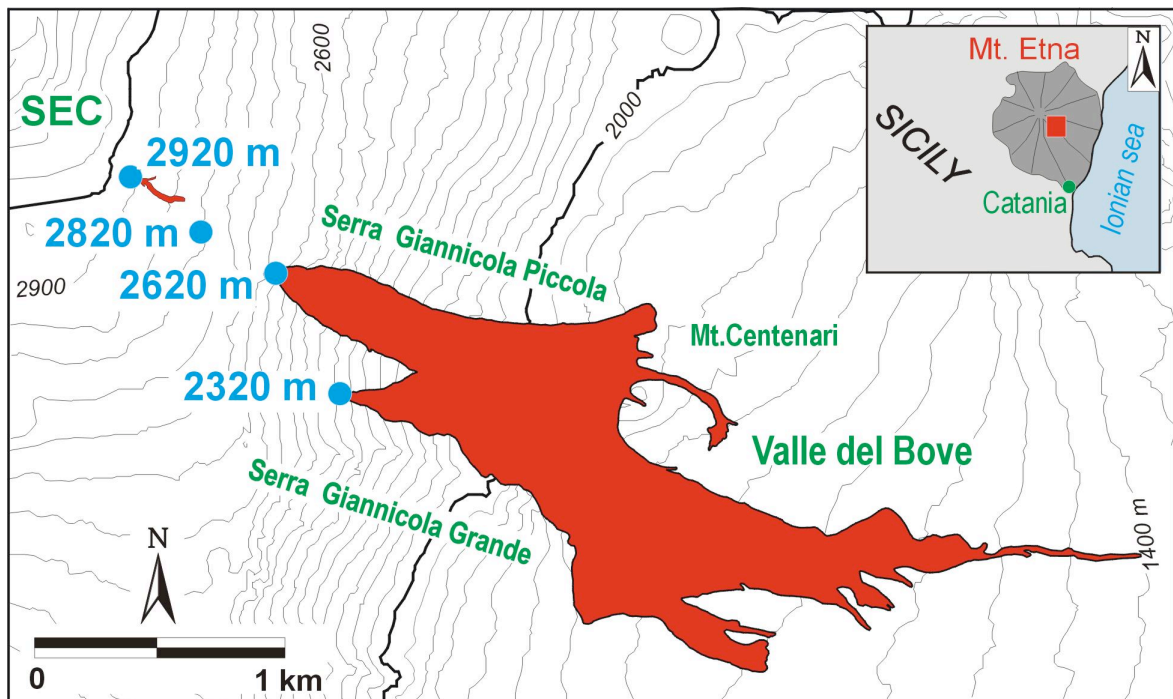




Fig. 6.17 Map of 2004/2005 eruptive fractures and lava fields. From Corsaro et al. 2009.

A new effusive vent opened at 2,620 m a.s.l. on September 10<sup>th</sup> and fed lava flow expanding towards the Serra Giannicola Piccola ridge (SGP) (Fig. 6.17). Then, the fracture zone propagated down slope and a new effusive vent opened at about 2,320 m a.s.l., close to Serra Giannicola Grande. After September 13<sup>th</sup>, the fracture zone did not evolve further, and the effusive activity was stabilized at both 2,620 and 2,320 m vents. During the next months, a compound lava field developed and reached about 1,600 m a.s.l. Complex lava tubes in the upper portion and several ephemeral vents in the central portion characterized the lava field. On March 8<sup>th</sup>, the eruption finished. The total volume of lava flows was estimated at  $40 \cdot 10^6$

m<sup>3</sup> by Neri and Acocella (2006) and 60\*10<sup>6</sup>m<sup>3</sup>.

#### 6.4.1 Petrographic features of emitted lavas

Corsaro et al., (2009), have performed a petrological study of emitted lavas. Plagioclase, clinopyroxene, olivine, and Ti-magnetite form the mineralogical assemblage of 2004–2005 lavas. The nature, abundance, relative proportions, and mineral chemistry of phenocrysts show a limited range of differences. Magma erupted on 25 February (SGP) is distinct for the higher clinopyroxene abundance (Table 6.4). All the analyzed samples show porphyritic texture. Porphyritic Index (total abundance of mineral phases) varies between 19.0 and 32.4 vol.%, and pl/mafic (plagioclase/(clinopyroxene + olivine + Ti-magnetite)) ranges from 0.8 to 2.1 (Corsaro et al. 2009). Plagioclase phenocrysts range between 1 and 3 mm in size, vary from 5.2 to 8.9 vol.%, and are mostly euhedral. Sieved and clear plagioclases frequently coexist in the same sample. Anhedral crystals are common among large plagioclase phenocrysts (see paragraph 6.4.3 for further details). Microphenocrysts are euhedral, ranging from 0.5 to 1 mm in size and vary from 4.5 to 6.8 vol.%. Phenocrysts and microphenocrysts have an average composition ranging from An<sub>84</sub> in the cores to An<sub>63</sub> at the rims. The composition of groundmass microlites (<100 μm) ranges An<sub>70–50</sub>. The average composition of microlites is An<sub>57</sub> and remains nearly constant throughout the eruption. (Corsaro et al. 2009).

Emission time	Magma type	Porphyritic index		Relative proportions of phenocrysts			Plagioclase texture	Type
		Range	Media	Cpx	OI	Plg		
2920 SEC	HKP	20-32	23.9	35-40	10-15	35-40		Type 1+4
2620-2320 SGP	HKP	19-19.4	19	45-50	20-25	10-15		Type 4+5

**Table 6.4** Petrographic features and plagioclase textures classification of 2004/2005 lavas.

Phenocrysts of clinopyroxene (4.3–10.5 vol.%) ranging from 1 to 5 mm across are euhedral and frequently enclose opaque minerals. The large crystals mostly show a zoning with the sectors of different Mg# ( $Mg/(Mg + Fe^{2+})$ ), whose average values are 0.73 and 0.78, respectively. Crystals with sector and oscillatory zoning are often observed in the same sample. Olivine phenocrysts (0.8–2.6 vol.%) range from 0.5 to 1 mm across. The large crystals are frequently resorbed, while the smallest ones are generally sub rounded in shape.

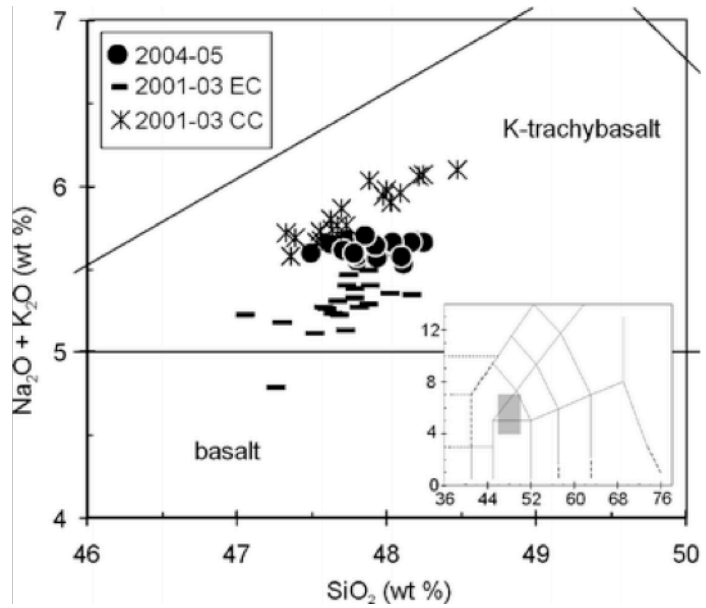


Fig. 6.18 TAS of lavas from 2004/2005. Samples from 2001 and 2002/2003 events are also reported for comparison. (Corsaro et al. 2009)

Olivine shows normal zoning from the core ( $FO_{80}$ ) to the rim ( $FO_{75}$ ), with the exception of large crystals with oscillatory zoning ( $FO_{73}$  core,  $FO_{76}$  intermediate zone,  $FO_{70}$  rim). Groundmass olivine microlites ( $<100 \mu m$ ) vary in composition from  $FO_{75}$  to  $FO_{68}$ . Scarce (0.1–1.5 vol.%) Ti-magnetite phenocrysts, ranging from 36 to 40 in Usp, are also present.

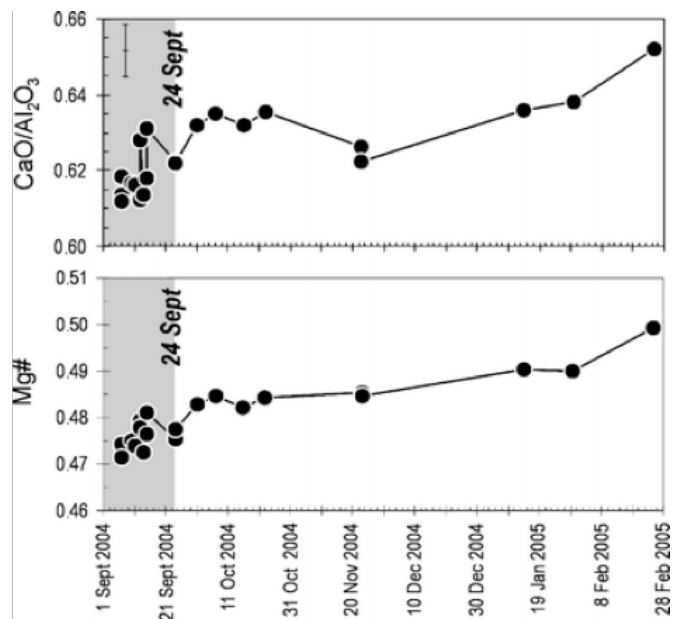


Fig. 6.19 Major element variations respect to the emission time.

Glomeroporphyritic clusters of mafic minerals are common in all samples. They are generally from 1 to 5 mm in diameter and are formed of 3–10 crystals of clinopyroxene, opaque oxides, and olivine in order

of abundance; glass pockets are also frequent between phenocrysts. Plagioclase is absent. The groundmass texture varies from glassy to hyalopilitic, consisting of brown glass, very few embedding plagioclase, and mafic minerals.

### 6.4.2 Geochemistry of whole rock

Products of the 2004–2005 eruption are trachybasalts (Fig. 6.18; Le Maitre 2002) with average  $\text{SiO}_2\% = 47.92 (\pm 0.19, 1\sigma)$  and  $(\text{CaO}/\text{Al}_2\text{O}_3 = 0.65$  and  $\text{Mg}\# = 0.50)$ .

Temporal variations of trace elements (Corsaro et al. 2009) reveal that most evolved magmas are erupted before September 24<sup>th</sup>. These lavas in fact show higher content of incompatible elements respectively. After September 24<sup>th</sup>, incompatible elements (e.g., Rb, La) of the lavas decrease, whereas compatible elements (e.g., Cr) increase. From 15 October up to the end of the eruption, most trace elements do not show significant variations.

The lavas erupted until September 24<sup>th</sup> are more enriched in incompatible elements and depleted in compatible elements than 2001–2003 CC and EC lavas (Corsaro et al. 2007; Fig. 6.20). After September 24<sup>th</sup>, the trace elements content

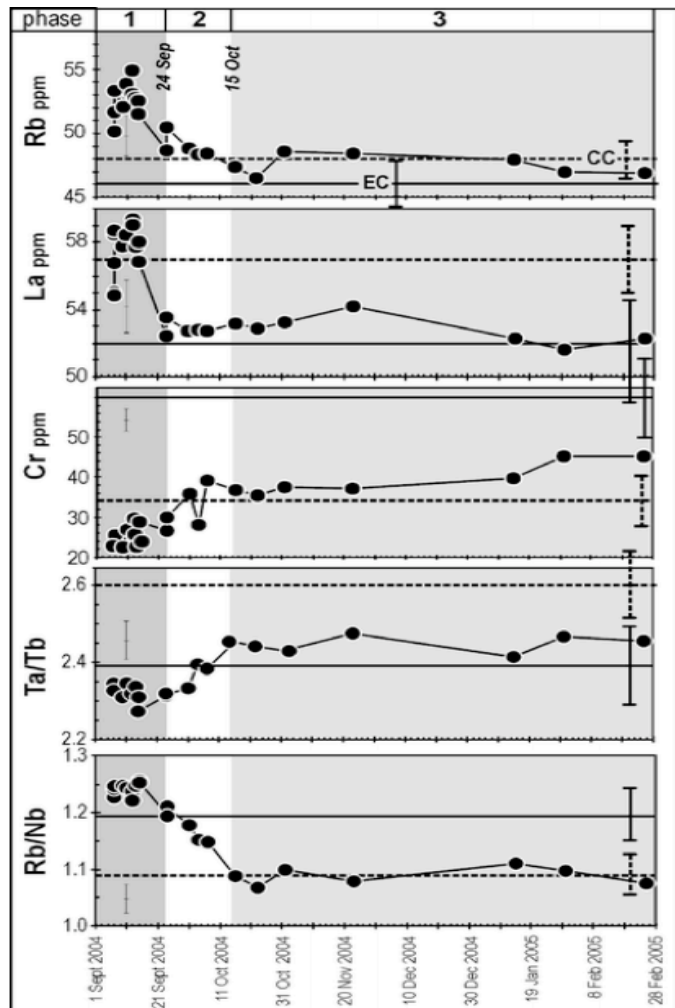


**Fig. 6.20** Trace elements variations respect to the emission time. (Corsaro et al. 2009)

overlaps between CC and EC products. The ratios of incompatible elements (Fig. 6.20), which hardly change through fractional crystallization (e.g., Ta/Tb) and are modified by contribution of aqueous fluids (e.g., Rb/Nb), clearly divide the 2004–2005 eruption into three phases: pre-24 September lavas (hereafter phase 1), characterized by the highest Rb/Nb and lowest Ta/Tb, lavas from 24 September to 15 October (phase 2) showing a decrease in Rb/Nb and increase in Ta/Tb, and post-15 October lavas (phase 3) with constant ratios in both Rb/Nb and Ta/Tb. (Fig. 6.20)

### ***6.4.3 Textures and compositional profiles of plagioclase***

Plagioclase in 2004/2005 eruption shows three main types of textures: plagioclase with oscillatory zonation (Type 1), plagioclase with coarsely sieved cores (Type 4) and plagioclase with resorbed dusty rims (Type 5).

Plagioclase embedded in lava emitted in first phase of the eruption from the fracture located at the SE flank of the South East Crater (SEC) are mainly Type 1 oscillatory crystals varying in composition from  $An_{86}$  to  $An_{78}$  at the cores, with a LAHF pattern and subordinately, Type 4 with coarsely sieved cores. No significant An variation has been recognized in relation to the sieved texture (Fig. 6.21 and 6.22). The frequency of appearance of Type 4 crystals increase with time. Plagioclases rims do not presents any significant texture and vary from in composition from  $An_{88}$  to  $An_{43}$ , strong anorthite depletion is observed at the outermost crystal rim.

Plagioclase emitted from the fracture at Serra Giannicola Piccola, from September 10<sup>th</sup> shows Type 4 textures and Type 5 resorbed dusty rims. Anorthite content varies from  $An_{85}$ - $An_{70}$  in the cores. Compositional profiles reveal an abrupt increase in An content ( $\Delta An \geq 10\%$ ) related to the resorbed rims (Fig. 6.21-6.22)

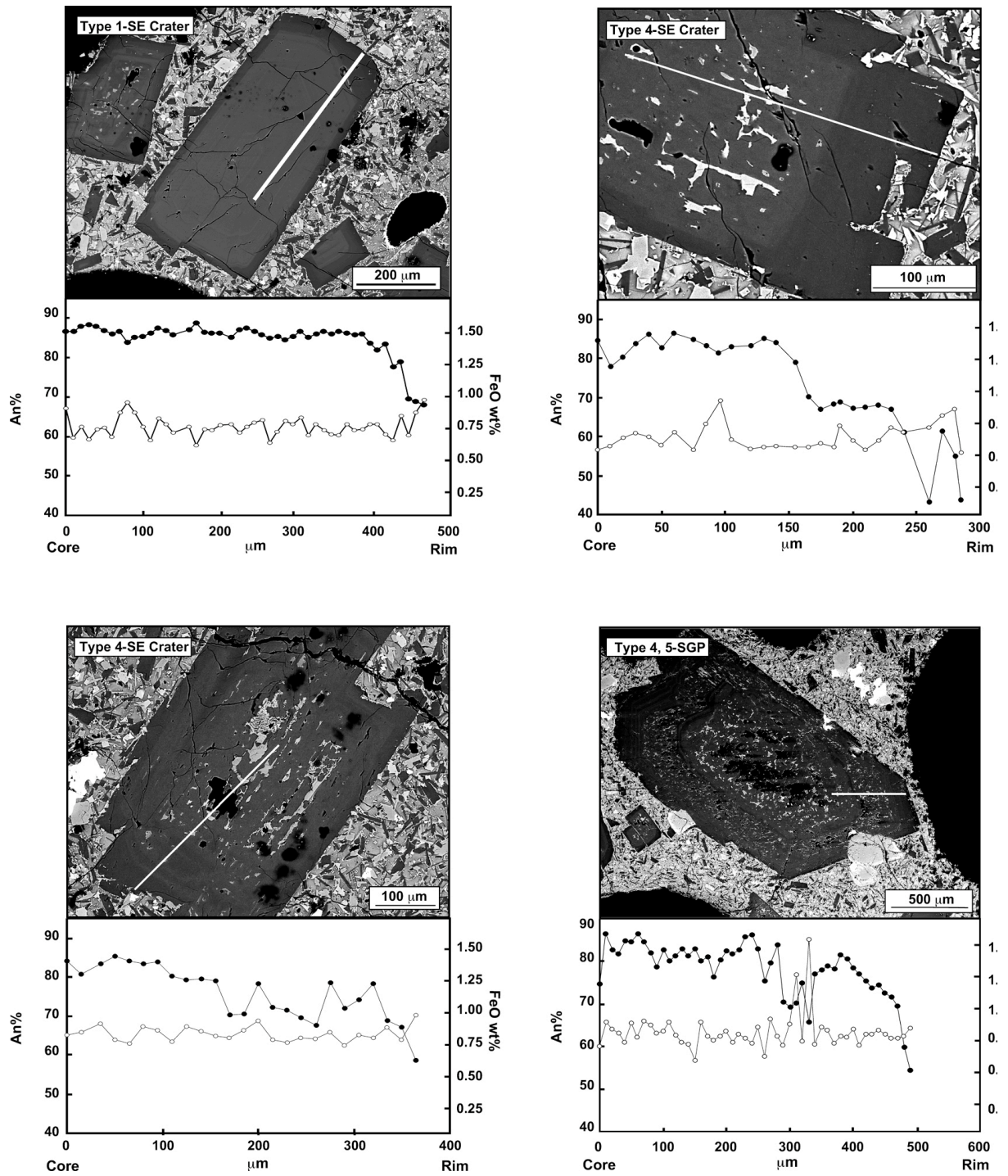


Fig. 6.21 Compositional profiles of An and FeO of plagioclase emitted during 2004 event.



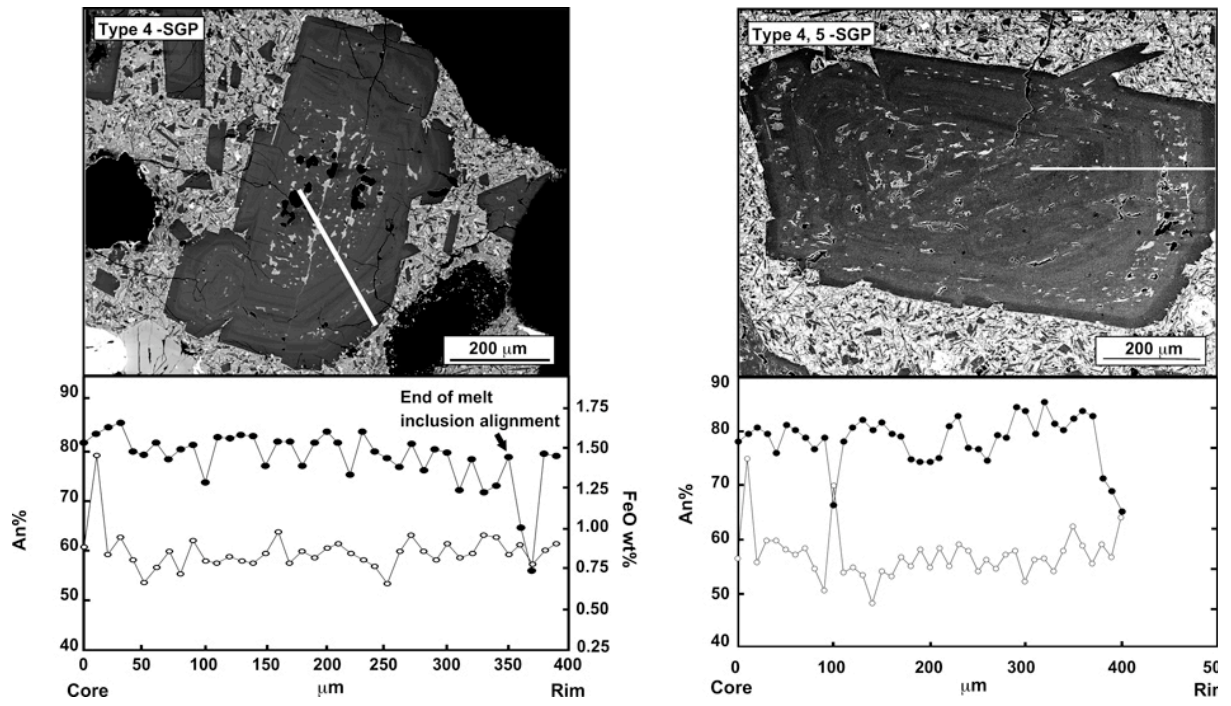
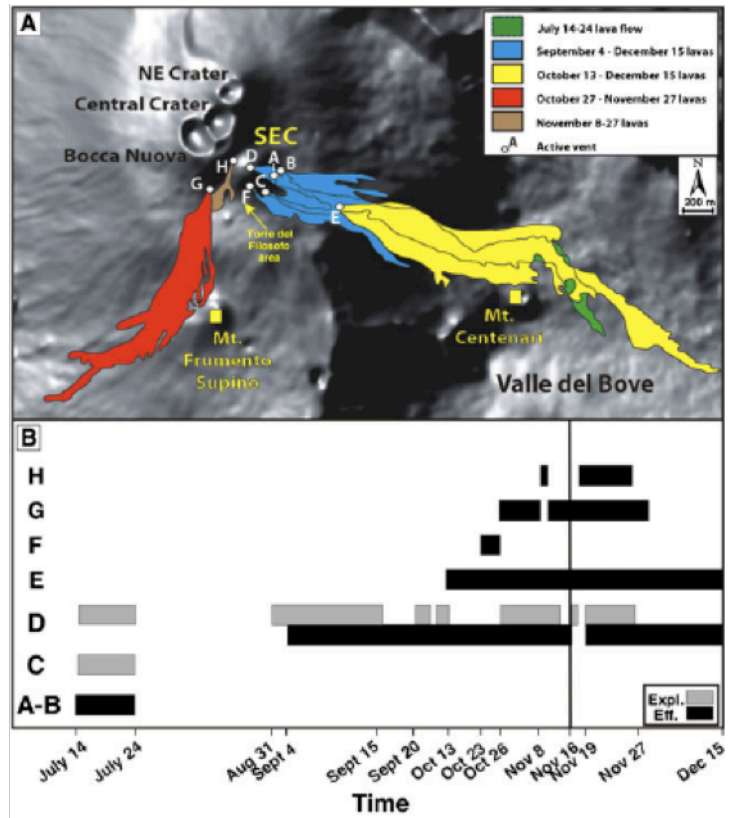


Fig. 6.22 Compositional profiles of An and FeO of plagioclase emitted during 2004 event.

## 6.5 2006 Eruptive event

Activity began after a period of rest lasting about 16 months, which followed the 2004–2005 eruption in the Valle del Bove. The activity of 2006 eruption has been studied in Ferlito et al. 2010. The first episode, on July 14, occurred on the eastern flank of the SEC at ~3050 m with two vents (labeled Vent A and B in Fig. 6.23) emitting lava flows at low rates ( $<5 \text{ m}^3/\text{s}$ ) that expanded into the Valle del Bove. On July 15, a third vent opened (Vent C; Fig. 6.23) at the highest tip of the fissure: this was characterized by strombolian activity with emission of lithics and juvenile ejecta. Over the following days (July 16–19), effusion continued regularly producing a compound lava field, extending for about 2.5 km in the Valle del Bove (Fig. 6.23) and a ~30-m-high cinder cone. In the evening of July 19, there was an abrupt change in the eruptive style: after a small collapse of the newly formed cone, explosive activity resumed, with dense clouds of scoriae and coarse blocks, while the emission rate increased ( $\sim 10 \text{ m}^3/\text{s}$ ) and lava overflowed the previously formed channel levees. From the morning of July 20, both the explosive and effusive activities decreased slightly, but in the evening the style changed from strombolian to sustained lava fountains reaching 250 m above the crater edge. From July 21 to 23 strombolian explosions lessened in frequency and lava flows were emitted at low rates ( $\sim 3 \text{ m}^3/\text{s}$ ). On July 24 the eruptive activity ceased, leaving a ~50-m-high scoria cone and a compound lava field extending for about 3 km down to ~1,700 m a.s.l. (Fig. 6.23).



**Fig. 6.23** a) DEM image (modified from Monaco et al. 2008) showing the lava fields relative to the eruptive period July–December 2006. Elevations of active vents: A, B, F, G=3,050 m; C=3,070 m; D=3,300 m; E=2,800 m; H=3,180 m. b) Time sequence and eruptive behaviour (effusive and/or explosive) at the active vents during 2006; labels as in Fig. 1° (Ferlito et al. 2010)

On August 31 the eruptive activity resumed at the SEC summit (Vent D in Fig. 6.23) with frequent strombolian explosions and emission of juvenile and lithic fragments. This activity,

mostly intra-crateric, continued until September 4 when lava overflowed from Vent D. This flow progressively filled the pit-crater formed during the 2004–2005 events on its eastern flank, and advanced eastward.

Both effusive and strombolian activities, with variable emission rates and intensity, characterized the period until September 15. During this interval, several rock-slides affected the eastern flank of the SEC edifice, which had already been destabilized by activity occurring during the late 2005 events and by those in July 2006 (cf. Behncke et al. 2009 and references therein). Only lava effusion at low emission rates ( $<1 \text{ m}^3/\text{s}$ ) occurred until September 20, when the explosive activity recommenced at Vent D, reaching maximum intensity on September 25. From October 3 to 13, activity was characterized by continuous lava flow emission accompanied by strombolian explosions varying in frequency and intensity. On October 13, a new vent opened at 2800 m (Vent E; Fig. 6.23), without explosive activity, emitting lava flows at  $\sim 3 \text{ m}^3/\text{s}$  directed toward the Valle del Bove. The eruptive scenario changed again on October 23: a new fissure opened at 3,050 m on the southern flank of the SEC cone (Vent F; Fig. 6.23), emitting flows at an average rate of  $\sim 10 \text{ m}^3/\text{s}$ . The explosive activity at the Vent D lasted, with varying frequency and intensity, until November 8. The activity at the new fissure ended on October 27, when a new effusive vent (Vent G; Fig. 6.23) opened at  $\sim 3,050 \text{ m}$  on the flank of the cone of the central crater (CC) just south of the Bocca Nuova, and poured out a SSW-directed flow at a rate of  $\sim 10 \text{ m}^3/\text{s}$ . On November 8, lava emission from Vent G ceased and lava was emitted for only one day from a new effusive vent (Vent H; Fig. 6.23) which opened next to the saddle between the SEC and the CC cones at  $\sim 3,180 \text{ m}$ . On November 9, lava emission from Vent G recommenced, while strombolian activity at Vent D and effusion at Vent E continued persistently (Fig. 6.23).

#### ***6.5.1 The paroxysm of November 16, 2006***

In the days before the paroxysm, several rock-slides involving blocks of some  $\text{m}^3$  in volume occurred at the south-eastern flank of the SEC cone (Ferlito et al. 2010). On the southern flank of the SEC cone a new N-S oriented fracture, 10 m long, 0.3 m wide, was observed (Fig. 3 in Ferlito et al. 2010). In the early morning of November 16, at around 5:00 UTC, the eastern sector of the SEC edifice began to be affected by rock sliding, while the volcanic tremor amplitude increased in intensity (cf. Behncke et al. 2009). At 6:15 UTC, eruptive activity began near the summit of the SEC with strong strombolian activity, accompanied by grey ash and steam explosions, and lava flows directed toward the Valle del Bove. At 14:00 UTC, a portion of the eastern flank of the cone had collapsed leaving a

horseshoe shaped niche, at the base (3,050 m a.s.l.) of which a gully ~250-m-long and ~15-m-deep developed (Fig. 6.24).



**Figure 6.24** a) Photo of the SEC cone taken from the Torre del Filosofo area in the afternoon of November 15. b) Photo of the SEC cone taken from the Torre del Filosofo area in the afternoon of November 16 after the paroxysm. Strombolian activity from the summit of the SEC cone and lava flow effusion into the niche continued after the paroxysm at 14.28 UTC. The base of the SEC is at ~3,050 and the summit at ~3,315 m a.s.l

Lava flows, which originated from a vent located about 50 m below Vent D at the SEC summit (~3,315 m; Fig. 6.24b), advanced within this gully and flowed for about 2 km further downslope into the Valle del Bove. The collapse was progressive and consisted of successive shallow slides accompanied by few major blocks movements. It is worth noting that the material involved in the slides was rafted by lava flows. Suddenly, at 14:28 UTC a few-meters-high billow of brown ash-laden steam was observed at the base of the niche (~3,050 m a.s.l.), immediately joined by another some 20 m upslope (Fig. 6.25). The billows evolved into ~150-m-high brownish plumes. These were immediately followed by an ESE-WNW oriented fracture opening along the gully (Fig. 3 in Ferlito et al. 2010) and a series of explosions which gave rise to a 300-m-high eruptive curtain, bearing juvenile and lithic clasts. From the RAI video filmed

by Giovanni Tomarchio, it is possible to observe at least 50 distinct explosions in the period of about 1 min (this video can be viewed at <http://etnalogos.net>).

The curtain was sustained for a short time (a little more than 1 min) and then collapsed, giving rise to a gravity driven pyroclastic flow, which moved downslope along the flank of the SEC down to ~2,800 m (Fig. 6.25). The flow advanced downwards, channeled into the gully described above, with relatively low (no more than 50-m-high) dark brown billows and accompanied by clouds of white steam which rose up to more than 500 m. Most of its deposit settled in the gully and was covered by lava flows in the following hours, whereas the elutriated fine-grained fraction extended for ~1.4 km

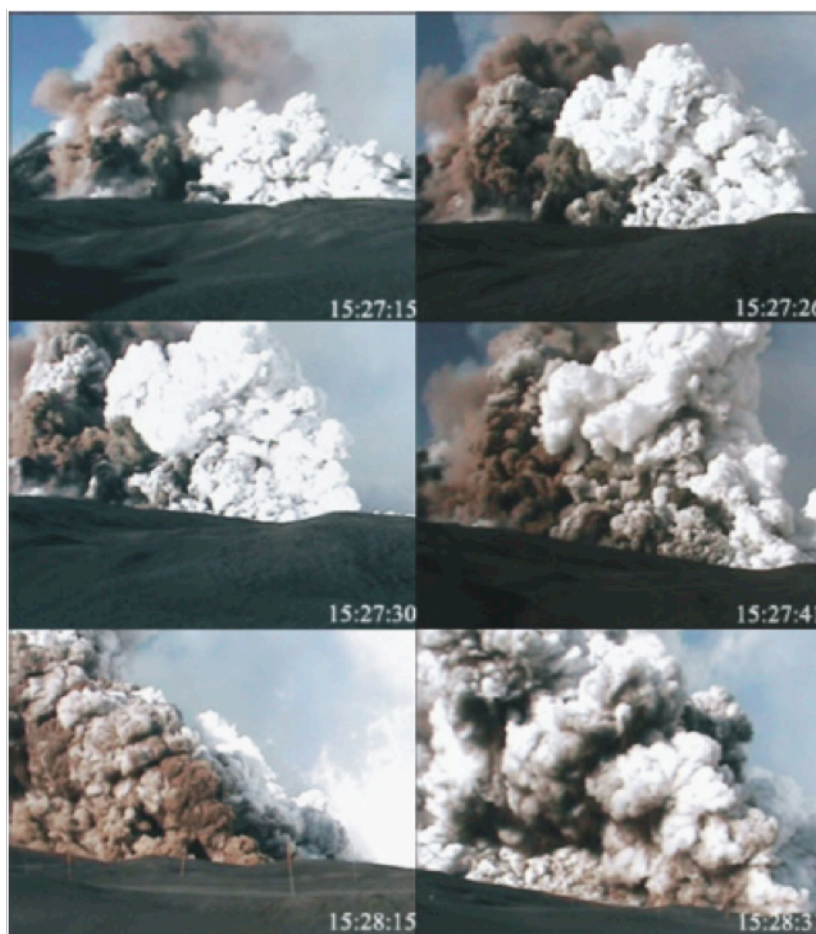


**Figure 6.25** Photos of the paroxysm of November 16, 2006 taken from the Torre del Filosofo area. The episode lasted no more than 2 min: specifically, the collapse of the eruptive curtain (h 15:27:41) with the development of pyroclastic flow (h 15:28:15) occurred about 1 min after the outburst from the fracture at the base of the SEC cone. Times in the pictures are Local (UTC+1 h) Ferlito et al. 2010.

downslope and covered an area of ~2 km<sup>2</sup> with an average thickness of ~2 cm (Figs. 3 and 6 in Ferlito et al. 2010). After this paroxysm, explosive activity continued at the SEC with decreasing intensity. Over the following hours, the exposed walls of the niche containing interlayered buried snow repeatedly fell onto the flowing lava, producing steam explosions due to the sudden vaporisation of the snow. Lava was emitted from the higher end of the eruptive fracture in the niche at 3,050 m (Fig. 3 in Ferlito et al. 2010) and flowed into the Valle del Bove. This activity continued until about 5:00 UTC on November 17.

After the November 16 peak, the eruption continued with alternating phases of effusive and strombolian activity. Four vents were fed at variable rates until the end of the eruption on December 15, 2006: specifically vents D, E, F and H (Fig. 6.23). Together with the effusive activity, the SEC showed phases of quiet fumarolic activity and episodes of violent ejections of

ash which produced sustained eruptive columns 4–5 km high, such as the paroxysm of November 24 (Behncke et al. 2009 and references therein). On November 27, lava effusion at Vents G and H ended. From then on, only vent E continued to emit lava and only episodic low-intensity strombolian activity occurred at the SEC. After about 2 weeks of emission at variable rates (generally  $<5 \text{ m}^3/\text{s}$ ), the 2006 eruptive events definitively ceased on December 15.

### ***6.5.2 Petrography and chemistry of the products***

#### **a) Tephra**

Six tephra samples of the pyroclastic flow deposit of November 16, 2006 were collected. Ferlito et al. 2010.

Fractions finer than 2 mm of these tephra were selected for morphologic investigation using a scanning electron microscope (SEM). The glass matrix of these grains was also chemically analyzed in order to determine major element compositions. The fragments analyzed were divided into three groups (Fig. 6.26): lithics, juvenile pyroclasts and hydroclasts. Lithics clasts, which constitute the largest group (~50% in volume; Fig. 6.26b), have polyhedral shapes with planar or sub-planar surfaces and can be interpreted as lava shards torn off from the fracture walls. Secondary minerals such as gypsum often fill the cavities (Fig. 6.26b).

Juvenile pyroclasts (Fig. 6.26c) constitute about 40% in volume of the deposit and are composed of shards and extremely vesiculated clasts (up to 50 vol% spheroid-ovoid bubbles). The petrographic analyses performed using optical and SEM, show that clasts are highly vesiculated and vitrophyric, with phenocrysts of plagioclase (bytownite to labradorite), augite, scarcer olivine and titaniferous magnetite (Porphyricity Index, PI ~25 vol%). In these clasts, sparse microlites with skeletal texture, which are mostly labradorite to andesine, constitute up to ~10% of total volume. Augite, scarce  $\text{Fo}_{73-72}$  olivine and titaniferous magnetite are also present. Phenocrysts and microlites are enclosed in limpid sideromelane, from light yellow to dark brown in colour. SEM-EDS data on sideromelane indicate a shoshonitic composition, according to Le Maitre (2002; Table 1 in Ferlito et al. 2010). This data compares well with the compositions of other glasses from recent eruptions [data from Ferlito et al. (2008) for the 2001 eruption; Spilliaert et al. (2006) for the 2002–2003 eruption; Corsaro and Miraglia (2005) for the 2004–2005 eruption], although they display the least evolved compositions compared to the reference glasses (Fig. 6.27a).

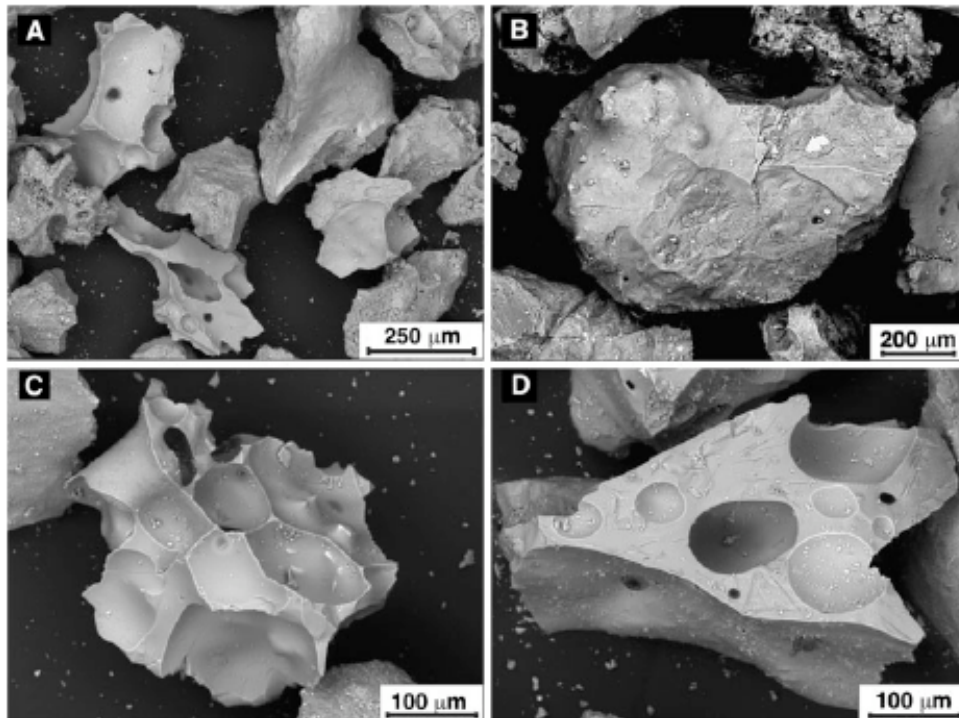


**Figure 6.26** a) Backscattered SEM image of some grains of the November 16 pyroclastic flow deposit; three types of clasts can be distinguished: b) lithic, c) juvenile, d) hydroclastic (Ferlito et al. 2010).

Finally, hydroclasts are angular and chunky in shape with ellipsoidal vesicles (~30 vol%) and conchoid surfaces (Fig. 6.26d). These constitute only a minor portion of the deposit (~10%), thus indicating that the quenching of magma with shallow depth groundwater and/or buried snow was a minor factor in the explosive activity that resulted in the opening of the eruptive fracture. Norini et al. (2009) also reported textural analyses of the deposit, confirming that lithics clasts are generally dominant with respect to the juvenile clasts, although with different percentages. However, they did not observe the presence of hydroclastic fragments.

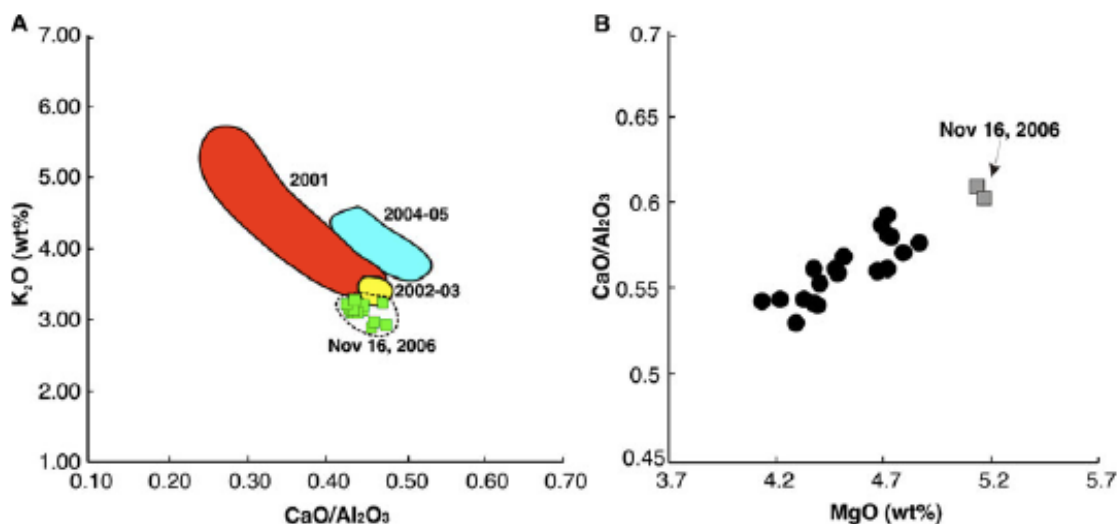


**Fig. 6.27** Major element variation for a residual glasses found in tephra grains of the November 16 pyroclastic flow deposit and b whole rocks of the July–December 2006 period. Comparison of residual glass compositions with glasses from tephra and lavas of recent eruptions highlights the rather primitive character of the July–December 2006 products, and particularly of those of the November 16 paroxysm [data source: Ferlito et al. (2008) for the 2001 eruption; Spilliaert et al. (2006) for the 2002–2003 eruption; Corsaro and Miraglia (2005) for the 2004–2005 eruption]. Note that whole rock compositions for the samples of lava emitted during the paroxysm of 14:28 UTC of November 16 are the most primitive of all 2006 products. (Ferlito et al. 2010)

## b) Lavas

Two samples of the lava emitted by the fracture opened at the base of the niche during the paroxysm of 14:28 UTC (Fig. 3 in Ferlito et al. 2010) were collected. Their petrography is similar to that of the lavas erupted from July to December 2006 and, in general, to that of the volcanic products from recent eruptions (cf. Viccaro and Cristofolini 2008). They are mesophyric with seriate texture and PI ~25 vol%. The most abundant phenocrysts are euhedral bytownite to labradorite (~10 vol%) and augite (~8 vol%), followed by euhedral to subhedral  $\text{Fo}_{83-75}$  olivine (~5 vol%) and scarcer titaniferous magnetite (~3 vol%). The groundmass varies from hyalopilitic to intersertal with variable amounts of glass. Microlites are mainly labradorite and subordinate augite, titaniferous magnetite and  $\text{Fo}_{72}$  olivine. Major element abundances of whole rocks were obtained at the Dipartimento di Scienze della Terra of the University of Calabria (Italy) using WD-XRF spectrometry. Generally, erupted products are trachybasalts (Le Maitre 2002), displaying throughout the 2006 period a slight variability not related to time. A notable feature is certainly represented by the more primitive character ( $\text{SiO}_2 < 47$  wt%;  $\text{MgO} > 5$  wt%) of the products erupted during the November 16 paroxysm, with respect to the volcanics of the entire 2006 period (Fig. 6.27). The primitive nature of the pulses of magma



feeding the activity during November 2006 would also account for the large amount of CO<sub>2</sub> involved in these paroxysmal events (cf. Aiuppa et al. 2007).

### ***6.5.3 Textural and compositional features of plagioclase***

Plagioclase embedded in lavas of 2006 eruption present Type 4, coarsely sieved cores and Type 5, resorbed dusty rim texture. Cores are bytownitic in composition (An<sub>87-80</sub>) evolving to rims of compositions varying from labradoritic to andesinic (An<sub>70-58</sub>).

Plagioclase differs in composition and texture type to respect to the emitting time. Phenocrysts in lavas emitted before and during November 16<sup>th</sup> are euhedral and presents resorbed dusty rims, composed by dense, partially recrystallized glass pockets (Fig. 6.28 a, b). Compositional profiles show a direct oscillatory LAHF pattern, interrupted by episodes of anorthite increase positively concordant to FeO variations. Crystals emitted before November 16<sup>th</sup> has An varying from An<sub>70</sub> and An<sub>88</sub> with several evident episode of calcic enrichment. However, most of the oscillations are from An<sub>80</sub> to An<sub>85</sub>. Cores in plagioclase emitted during November 16<sup>th</sup> are quite more calcic, ranging from An<sub>90-80</sub>. Resorbed dusty rims are frequent in both lavas, and are associated to strong An and FeO (~ΔAn 15%) increase while the outermost rims shows a strong anorthite drop.

Plagioclase emitted in lavas after the November 16<sup>th</sup> episode are euhedral and shows type 4 texture, characterized by coarsely sieved cores (Fig. 6.28 c). Compositional profiles show an oscillatory pattern both HALF and LAHF. Wide amplitude oscillations (An<sub>86-73</sub>) are constant along the profile, and no significant variations are associated to the coarsely sieved textures. Compositions are bytownitic in average, trending toward labradoritic at the rims. As most off etnean plagioclases an An drop is observed very close to the outermost rims.

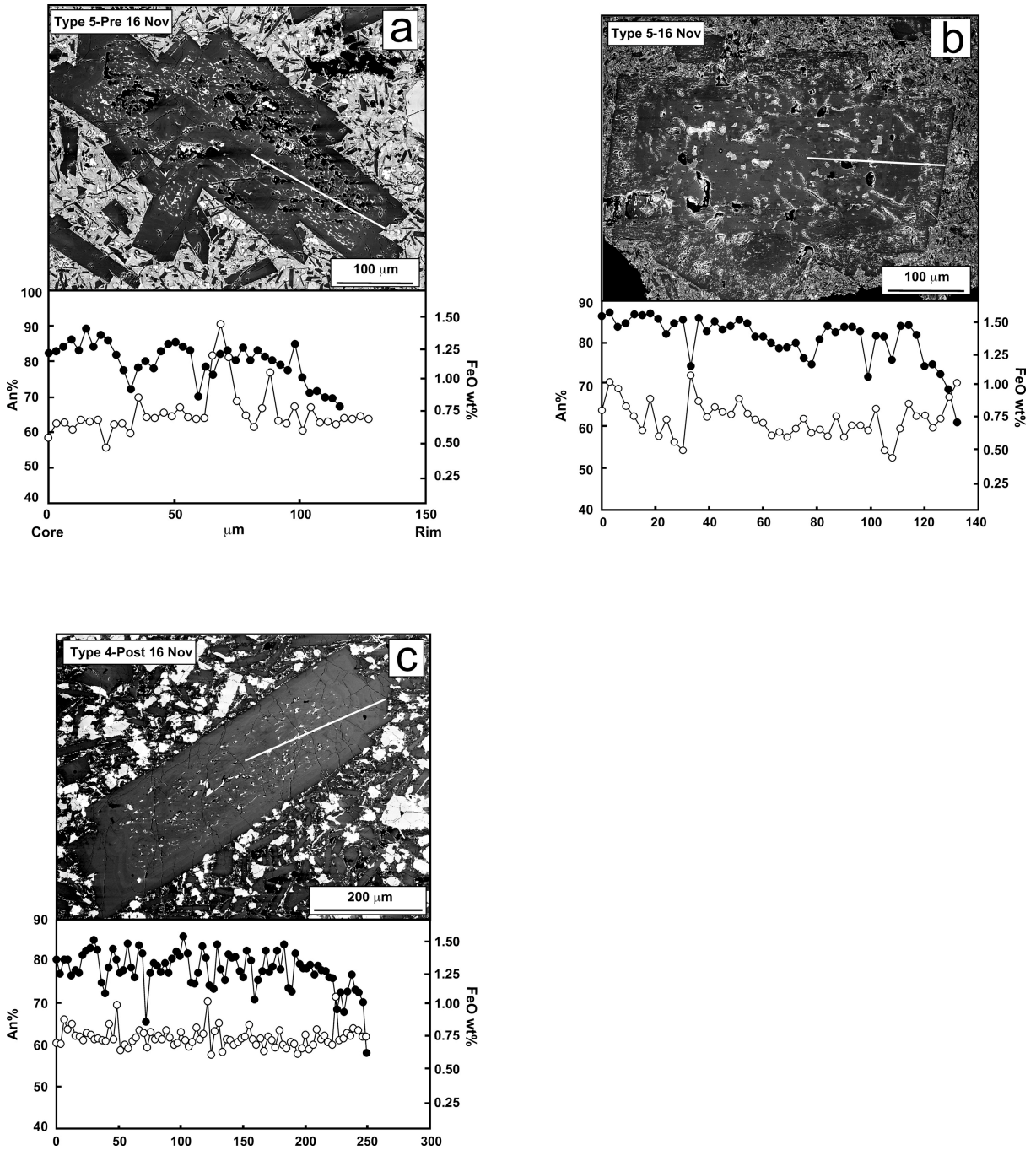


**Fig. 6.28** Compositional profiles of An and FeO of plagioclase emitted during 2006 event.